J|A|C|S
ARTICLES

Published on Web 05/05/2010

Total Synthesis and Structural Revision of Vannusals A and B: Synthesis of the True Structures of Vannusals A and B

K. C. Nicolaou,* Adrian Ortiz, Hongjun Zhang, and Graziano Guella†

Department of Chemistry and the Skaggs Institute for Chemical Biology, The Scripps Research Institute, 10550 North Torrey Pines Road, La Jolla, California 92037, and the Department of Chemistry and Biochemistry, University of California, San Diego, 9500 Gilman Drive, La Jolla, California 92093

Received February 1, 2010; E-mail: kcn@scripps.edu

Abstract: Having determined through total synthesis that the originally assigned structure of vannusals A and B were incorrect, we set out to uncover the identity of the true structures of these novel marine natural products. Our search was based on intelligence gathered by NMR spectroscopy and chemical synthesis and took us through the total synthesis of eight diastereomeric vannusal B structures [**2**, **d-2**, **3**, **d-3**, **4**, **d-4**, **5**, and **d-5**, Figure 2]. The true structures of vannusals A and B were finally determined to be **d-5** and **d-1**, respectively. Their total synthesis was based on a highly convergent and efficient strategy that involved fragments vinyl iodide (−)-**6** and aldehyde (±)-**94**, and featured a stereoselective lithium-mediated coupling reaction and a samarium-induced cyclization process that forged the final ring of the carbon framework. The synthetic strategies and technologies developed in these investigations expand the scope of chemical synthesis and render these compounds readily available for biological evaluation, while the NMR spectroscopic insights gained should prove useful in future structural determination endeavors.

Introduction

In the preceding article[1] we described the total synthesis of the originally assigned structure of vannusal B, one of two marine natural products whose isolation and structural assignment [structures **1** (vannusal A) and **2** (vannusal B), Figure 1] were reported in 1999, by Guella, Dini, and Pietra.[2] Comparison of the NMR spectral data of synthetic **2** and natural vannusal B revealed the nonidentity of the originally assigned structure (**2**) to the true structure of vannusal B, precipitating a structural puzzle whose solution was exacerbated by the scarcity of the natural products. In this article, we present a detailed account of our work that led to the demystification of this conundrum and, at the same time, the total synthesis of vannusals A and B and several of their analogues.

Results and Discussion

Despite its failure to prove the structure of vannusal B, our total synthesis of the originally assigned structure (+)-**2**[1,3] provided a wealth of information in terms of synthetic technology and NMR spectroscopic intelligence that proved invaluable in our campaign to elucidate the true structures of the vannusals, a campaign that required the total synthesis of eight vannusal B diastereoisomers (**2**, **d-2**, **3**, **d-3**, **4**, **d-4**, **5**, and **d-5**, Figure 2). Figure 3 shows the well-resolved and diagnostic region (δ 5.7−3.5 ppm) of the ^{1}H NMR spectra of the synthetic, originally assigned, vannusal B structure [(+)-**2**] (top) and natural vannusal B (bottom). As seen from comparing the two spectral regions, the most dramatic discrepancy lay with H_{26} ($\Delta\delta$ +0.485 ppm). Panels a and b of Figure 4 depict the ^{1}H and ^{13}C NMR chemical shift differences, respectively, between the synthetic, originally assigned, vannusal B structure (+)-**2** (blue bars) and natural vannusal B (set to zero).

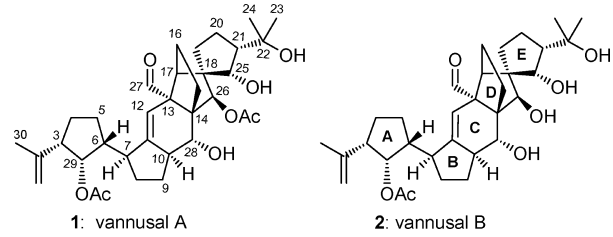

Figure 1. Originally assigned structures of vannusals A (**1**) and B (**2**).

While the ^{1}H NMR comparison (Figure 4a, blue bars) reveals several chemical shift differences, two stand out: those of H_{26} (mentioned above and seen in Figures 3 and 4a) and $H_{16right}$ (seen in Figure 4a) ($\Delta\delta$ −0.413). The fact that both these protons were located in the "northeastern" domain of the molecule, together with the realization that most differences resided in the same region, pointed to the vicinity around rings D and E as the problematic site of the structure. This assumption was further supported by similarly large differences in the ^{13}C NMR chemical shifts (Figure 4b, blue bars), most notably for C_{21} ($\Delta\delta$ −11.54 ppm), C_{25} ($\Delta\delta$ +3.91 ppm), and C_{27} ($\Delta\delta$ +3.00 ppm). Interestingly, the synthetic diastereomeric structure (+)-**d-2** exhibited less drastic differences both in its ^{1}H (Figure 4a, red bars) and ^{13}C NMR (Figure 4b, red bars) spectra from natural

† Faculty of Science, Bioorganic Chemistry Lab, University of Trent, Italy.

(1) Nicolaou, K. C.; Ortiz, A.; Zhang, H.; Dagneau, P.; Lanver, A.; Jennings, M. P.; Arseniyadis, S.; Faraoni, R.; Lizos, D. E. *J. Am. Chem. Soc.* **2010**, *132*, DOI: 10.1021/ja100740t (preceding article).
(2) Guella, G.; Dini, F.; Pietra, F. *Angew. Chem., Int. Ed.* **1999**, *38*, 1134–1136.
(3) Nicolaou, K. C.; Zhang, H.; Ortiz, A.; Dagneau, P. *Angew. Chem., Int. Ed.* **2008**, *47*, 8605–8610, see also ref 1.

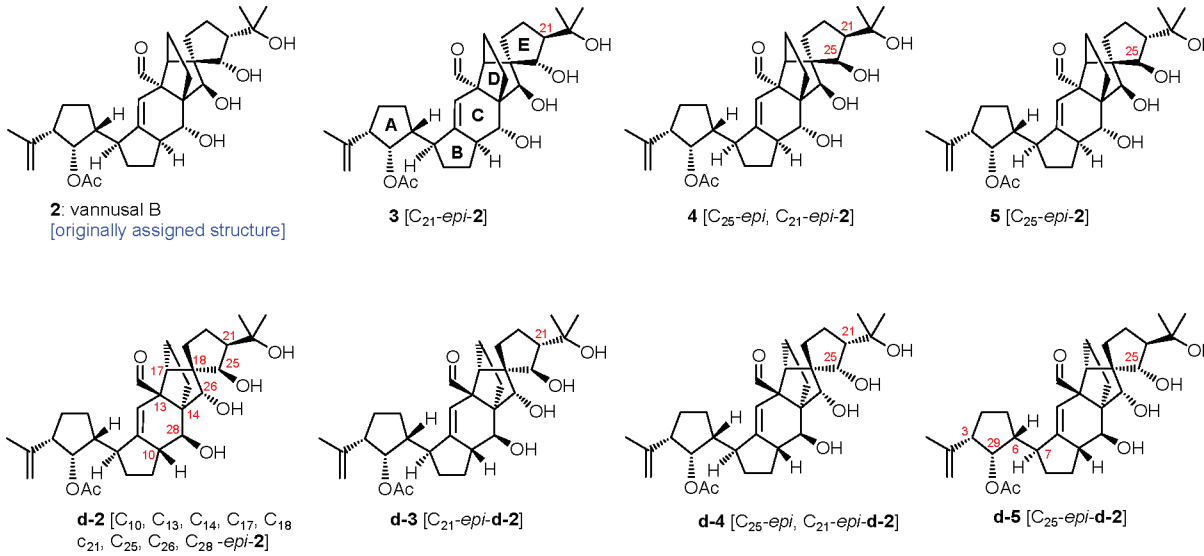

Figure 2. Vannusal B structures (**2**, **d-2**, **3**, **d-3**, **4**, **d-4**, **5**, and **d-5**) synthesized as part of the campaign to elucidate the true structures of the vannusals.

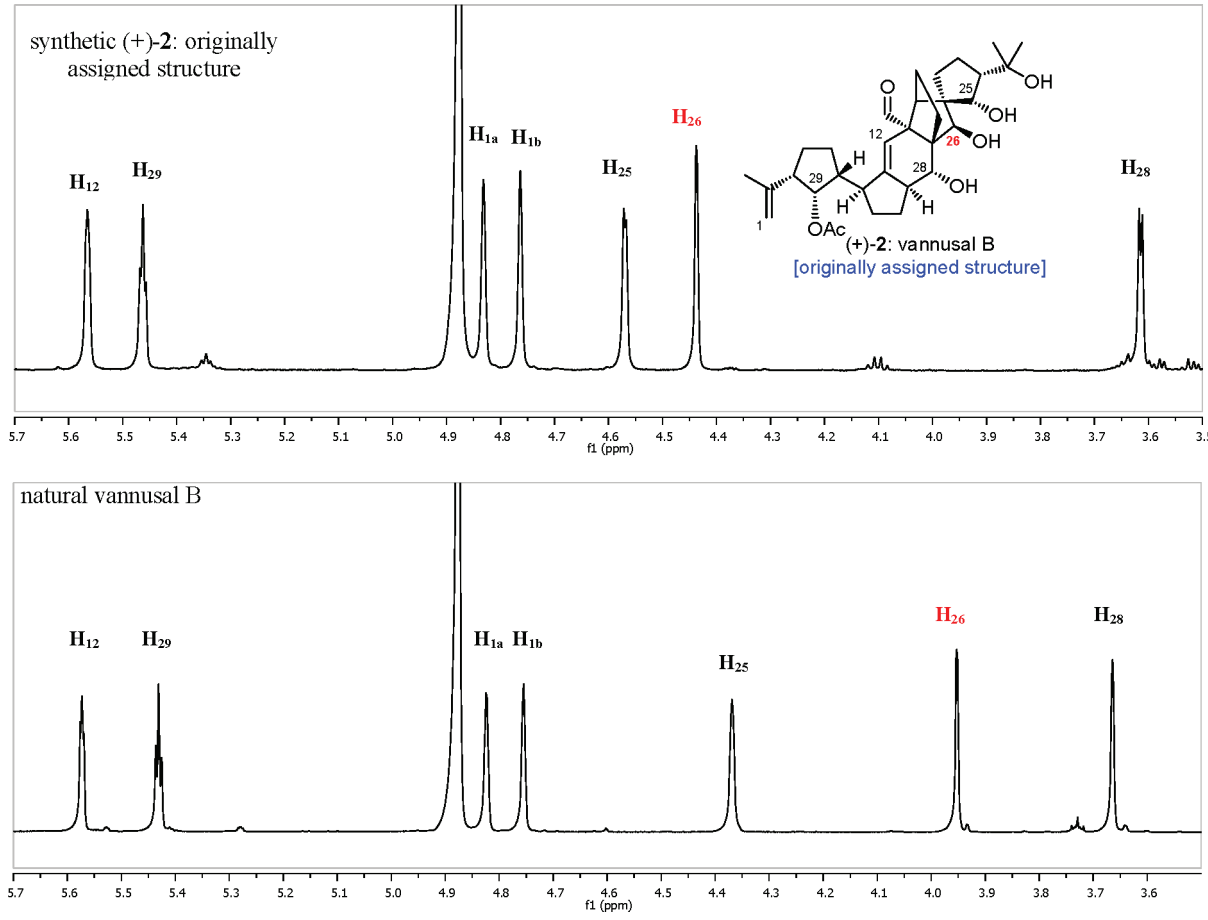

Figure 3. ^{1}H NMR spectral comparison (δ 5.7−3.5 ppm, d_4-MeOH, 4600 MHz) of the originally assigned structure [(+)-**2**, top] and natural vannusal B (bottom).

vannusal B. Having convinced ourselves of the general vicinity of the problem and that the originally assigned overall skeleton of the molecule was correct, we then attempted to pinpoint the correct configuration(s) of the stereocenter(s) within the "north-eastern" region of the vannusal B structure. For this we relied on the NMR spectroscopic evidence shown in Figure 5, which included: (a) a revealing *w*-*J* coupling between H_{26} and H_{15left} present in both synthetic and natural vannusal B (*w*-$JH_{26,15left}$ = 1.6 Hz); (b) NOEs between H_{26} and H_{27}, and H_{26} and $H_{19\alpha}$; and (c) NOE between H_{25} and $H_{16right}$. The first two observations (a and b) provided evidence for the correctness of the initial configurational assignment at C_{26}, whereas the latter observation (c) supported the originally assigned configuration of the C_{18} stereocenter.[2]

Faced with this evidence we focused our search on a possible configurational error at C_{25} and/or C_{21}. Indeed, the

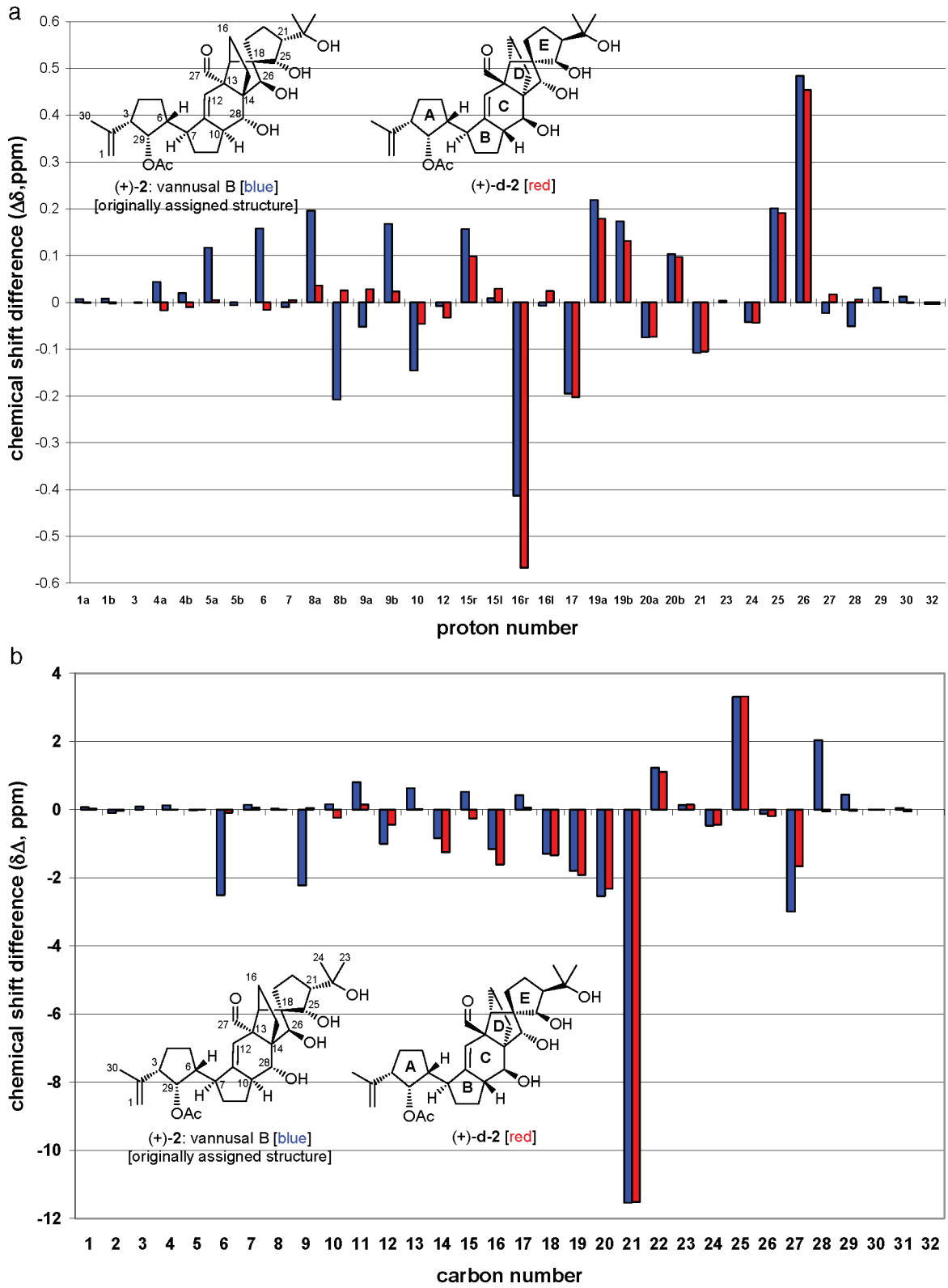

Figure 4. (a) Graphically depicted ^{1}H chemical shift differences ($\Delta\delta$, ppm, d_4-MeOH, 600 MHz) between the originally assigned structures [(+)-**2**: blue and (+)-**d-2**: red] and natural vannusal B (set to zero). r = right; l = left. (b) Graphically depicted ^{13}C chemical shift differences ($\Delta\delta$, ppm, d_4-MeOH, 600 MHz) between the originally assigned structures [(+)-**2**: blue and (+)-**d-2**: red] and natural vannusal B (set to zero).

spectroscopic evidence upon which the original configurational assignment at these stereocenters relied was incomplete.[2] The fact that these stereocenters resided on a cyclopentane ring made their assignment even more treacherous, as revealed from the observation of seemingly conflicting coupling constants for natural vannusals A [$JH_{25,21}$ = 6.6 Hz (d_4-MeOH) or 8.3 Hz (d_6-benzene)] and B [$JH_{25,21}$ = 2.0 Hz (d_4-MeOH)].[2] Our synthetic vannusal B structure (+)-**2** exhibited $JH_{25,21}$ = 3.0 Hz (d_4-MeOH). In deciding which one of the three remaining C_{25}/C_{21} diastereoisomers of the

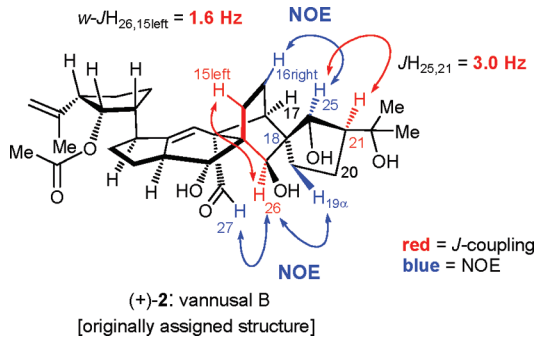

Figure 5. Key ^{1}H NMR coupling constants and NOEs exhibited by both the originally assigned structure [(+)-**2**] and natural vannusal B.

originally assigned vannusal B structure [(+)-**2**] to be the next synthesized, we were influenced by the hemi-vannusal biosynthetic hypothesis proposed by Guella et al. and summarized in Figure 6.[4]

Thus, assuming that two molecules of the same absolute configuration of hemivannusal are joined and processed to vannusal B, and that no epimerization takes place along the biosynthetic pathway, then the C_{21} absolute configuration of the product should be the same as its C_3 absolute configuration [3(*S*)], namely 21(*S*) (see Figure 6). It was on the basis of this hypothesis that we chose structure (+)-**3** [C_{21}-*epi*-**2**] as our next synthetic target, hoping that it would be the true structure of vannusal B.

Total Synthesis of Vannusal B Structure (+)-3 [C_{21}-epi-2]. The synthetic strategy employed to synthesize vannusal B structure (+)-**3** [C_{21}-*epi*-**2**] was based on the same retrosynthetic analysis that was used to design the total synthesis of the originally assigned structure (+)-**2**.[1,3] In this case, this analysis defined vinyl iodide (−)-**6** and aldehyde fragment (±)-**7** as the required building blocks (see Figure 7). Since the vinyl iodide [(−)-**6**] was already available through a previously developed route,[1,3] the immediate goal for this synthesis was to develop a process for the construction of aldehyde (±)-**7**. To this end, and after a few scouting expeditions, we devised a diastereoselective synthesis of nitrile acetonide (±)-**14** (Scheme 1) which served as a precursor to the desired aldehyde (±)-**7** (Scheme 2). Thus, Martin's sulfurane-induced dehydration of diol (±)-**8**[5] led to hydroxy olefin (±)-**9** (87% yield, Scheme 1), which was subjected to vanadium-catalyzed epoxidation [*t*-BuOOH, $VO(acac)_2$ (cat.)][6] to afford regio- and diastereoselectively epoxide (±)-**10** (90% yield, single diastereomer). Postulated transition state **9-TS** explains the selectivity of this reaction (homoallylic assistance). Reaction of hydroxy epoxide (±)-**10** with the Nagata reagent (Et_2AlCN) failed to produce the desired dihydroxy nitrile (±)-**13** in satisfactory yield, instead leading to a dihydroxy ethyl-containing compound as a major product.

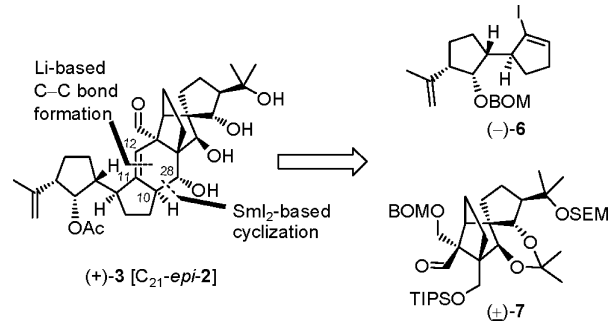

Figure 7. Retrosynthetic analysis of vannusal B structure (+)-**3** [C_{21}-*epi*-**2**].

Therefore, a short detour was necessary to reach the desired dihydroxy nitrile intermediate. Reasoning that the side reaction was occurring through initial formation of an R-$OAlEt_2$ species followed by intramolecular delivery of an Et group, we proceeded to block the free hydroxyl with an acetate group (Ac_2O, Et_3N, 4-DMAP, 90%) to generate acetate epoxide (±)-**11**, whose reaction with Et_2AlCN occurred as anticipated in 81% yield to afford the expected hydroxy acetate (±)-**12**. Removal of the now superfluous acetate group (K_2CO_3, MeOH, quant.) from this hydroxy acetate furnished the targeted dihydroxy nitrile (±)-**13** as a single compound. Acetonide formation [$(MeO)_2CMe_2$, PPTS] then led to crystalline acetonide nitrile (±)-**14** (mp 87−88 °C, hexanes, 89% yield). X-ray crystallographic analysis of the latter compound provided unambiguous confirmation of its structure (see ORTEP, Scheme 1, bottom).[7] The required aldehyde fragment (±)-**7** was synthesized from nitrile acetonide (±)-**14** as summarized in Scheme 2. To this end, the nitrile group of (±)-**14** was converted to the desired tertiary alcohol moiety through a high-yielding, four-step procedure involving (a) aldehyde generation (DIBAL-H), (b) MeMgBr addition, (c) oxidation [NMO, TPAP, (cat.)],[8] and (d) a second MeMgBr addition to afford intermediate (±)-**15** in 80% overall yield. The latter was then protected with SEMCl in the presence of *i*-Pr_2NEt and *n*-Bu_4NI to give the corresponding SEM ether acetonide, whose terminal olefin was cleaved (O_3; Ph_3P), furnishing the expected aldehyde (91% over the two steps). The latter reacted with allyl chloride in the presence of KH to afford the desired allyl enol ether (±)-**16** (95% yield, *E*:*Z* ~6:1). Heating of this enol ether under microwave conditions (200 °C) induced the expected Claisen rearrangement, furnishing upon $NaBH_4$ reduction primary alcohol (±)-**17** (97% overall yield). With the last quaternary center installed, protection of the hydroxyl group within the latter compound as a BOM ether (BOMCl, *i*-Pr_2NEt, *n*-Bu_4NI), followed by ozonolytic cleavage (O_3; Ph_3P, 80% yield for the two steps) of the terminal olefin, led to aldehyde (±)-**18**, which was then truncated to the desired aldehyde (±)-**7** through a two-step sequence involving

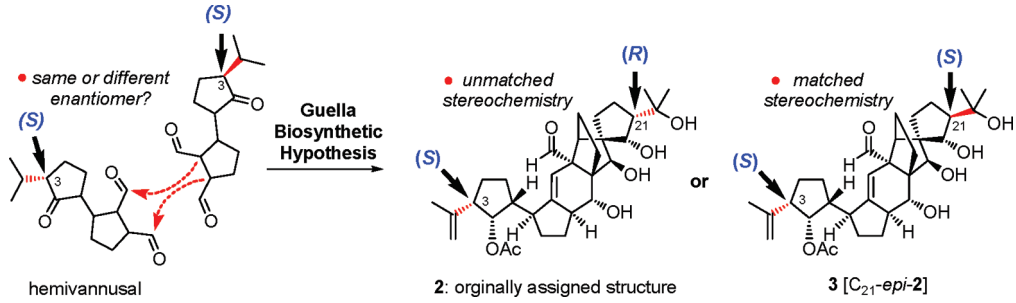

Figure 6. Guella biosynthetic hypothesis for the vannusals providing impetus for targeting vannusal B structure (+)-**3** [C_{21}-*epi*-**2**].[4]

Scheme 1. Construction of Nitrile Acetonide (±)-**14** (top) and Its X-ray Derived ORTEP (bottom)[a]

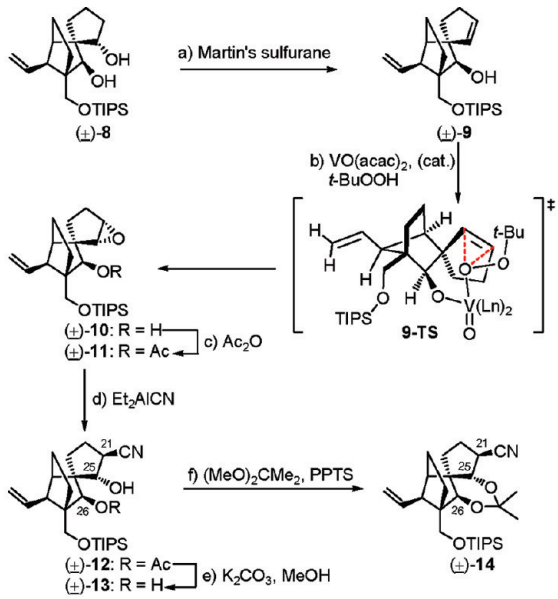

[a] Reagents and conditions: (a) Martin's sulfurane (1.1 equiv), Et_3N (10 equiv), CH_2Cl_2, 25 °C, 5 h, 87%; (b) *t*-BuOOH (3.0 equiv), $VO(acac)_2$ (0.2 equiv), benzene, 25 °C, 6 h, 90%; (c) Ac_2O (10 equiv), Et_3N (30 equiv), 4-DMAP (1.0 equiv), CH_2Cl_2, 4 h, 25 °C, 90%; (d) Et_2AlCN (10 equiv), toluene, −78 → −20 °C, 19 h, 81%; (e) K_2CO_3 (1.0 equiv), MeOH, 25 °C, 2 h, quant.; (f) DMF/2,2-dimethoxypropane (1:1), PPTS (1.0 equiv), 24 h, 89%.

Scheme 2. Construction of Aldehyde (±)-**7**[a]

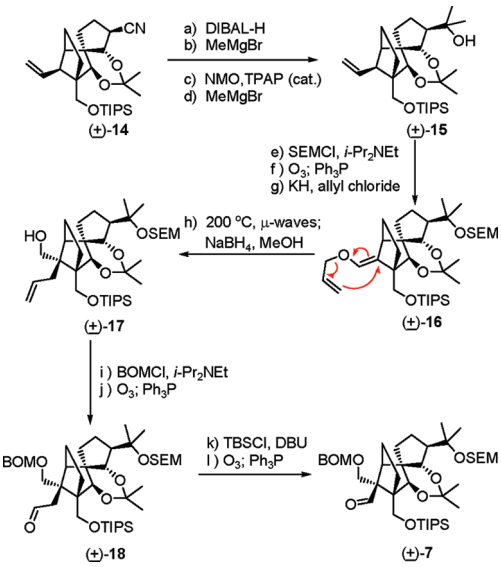

[a] Reagents and conditions: (a) DIBAL-H (1.5 M in toluene, 1.15 equiv), toluene, −78 → −20 °C, 1 h; then 0.1 N aq HCl, 25 °C, 30 min; (b) MeMgBr (5.0 equiv), THF, 0 °C, 1 h; (c) NMO (2.0 equiv), TPAP (0.05 equiv), CH_2Cl_2; MeCN (9:1), 25 °C, 1 h; (d) MeMgBr (5.0 equiv), THF, −10 °C, 1 h, 80% for the four steps; (e) *n*-Bu_4NI (1.0 equiv), SEMCl (5.0 equiv), *i*-Pr_2NEt (20 equiv), 12 h; (f) O_3, py (1.0 equiv), CH_2Cl_2/MeOH (1:1), −78 °C; then Ph_3P (5.0 equiv), −78 → 25 °C, 1 h, 91%; (g) KH (10 equiv), allyl chloride (20 equiv), HMPA (10 equiv), DME, −10 → 25 °C, 8 h, 95% (*E*:*Z* ∼6:1); (h) *i*-Pr_2NEt (1.0 equiv), *o*-dichlorobenzene, 200 °C (μ-waves), 20 min; then $NaBH_4$ (10 equiv), MeOH, 2 h, 25 °C, 97% for the two steps; (i) BOMCl (10 equiv), *i*-Pr_2NEt (30 equiv), *n*-Bu_4NI (1.0 equiv), CH_2Cl_2, 50 °C 12 h; (j) O_3, py (1.0 equiv), CH_2Cl_2/MeOH (1:1), −78 °C; then Ph_3P (5.0 equiv), −78 → 25 °C, 1 h, 80% for the two steps; (k) TBSCl (10 equiv), DBU (20 equiv), CH_2Cl_2, 25 °C, 24 h; (l) O_3, py (1.0 equiv), CH_2Cl_2/MeOH (1:1), −78 °C; then Ph_3P (5.0 equiv), −78 → 25 °C, 1 h, 86% for the two steps.

enol ether formation (TBSCl, DBU) and ozonolytic cleavage (O_3; Ph_3P, 86% overall yield).

With both fragments, vinyl iodide (−)-**6** and aldehyde (±)-**7** available, their union became the next task. Thus, and as shown in Scheme 3, lithiation of vinyl iodide (−)-**6** (*t*-BuLi, −78 → −40 °C) followed by addition of aldehyde (±)-**7** led to the expected coupling products (∼1:1 dr), which after desilylation with TBAF were chromatographically separated to afford pure diastereomers (−)-**19** (35% yield) and (−)-**20** (30% yield). The conversion of diastereomer (−)-**19** to cyclization precursor (−)-**21** required four steps, namely: (i) temporary silylation (TESCl, imid.); (ii) carbonate formation (KHMDS, $ClCO_2Me$, Et_3N, −78→25 °C); (iii) selective desilylation (HF·py/py, 0 → 25 °C, 90% overall yield); and (iv) oxidation [$PhI(OAc)_2$, TEMPO, 87%]. Disappointingly, however, the much anticipated cyclization of aldehyde carbonate (−)-**21** under the standard SmI_2-conditions failed to produce either of the expected polycyclic systems (**23α/β**). Interestingly, when the diastereomeric aldehyde carbonate (−)-**22** [prepared through the same sequence as (−)-**20** as shown in Scheme 3] was subjected to the same cyclization conditions (SmI_2, HMPA, −10 → 25 °C), the reaction proceeded well, furnishing polycyclic system (−)-**24** in 76% yield and as a single diastereomer. Despite this rather intriguing observation, we failed to derive any insightful information from it at this stage and returned to our objective of elaborating what we perceived at the time to be the correct diastereomeric coupling product [i.e., (−)-**19**] to the desired polycyclic structures through a more favorable cyclization substrate. In retrospect, as we shall see later, a subtle clue was hidden within these observations; specifically, we refer to the meaning of the failure of (−)-**21** to undergo ring closure and the facility by which (−)-**22** cyclized readily to form the desired product with correct configurations at both newly generated stereocenters.

Our return to the drawing board soon led to the adoption of a plan to modify the cyclization substrate so as to take advantage of our previous findings in connection with the synthesis of the

(4) Guella, G.; Callone, E.; Di Giuseppe, G.; Frassanito, R.; Frontini, F. P.; Mancini, I.; Dini, F. *Eur. J. Org. Chem.* **2007**, 5226–5234.
(5) Arhart, R. J.; Martin, J. C. *J. Am. Chem. Soc.* **1972**, *94*, 4997–5003. Arhart, R. J.; Martin, J. C. *J. Am. Chem. Soc.* **1972**, *94*, 5003–5010.
(6) Mihelich, E. D.; Daniels, K.; Eickhoff, D. J. *J. Am. Chem. Soc.* **1981**, *103*, 7690–7692.
(7) CCDC-726953 contains the supplementary crystallographic data for (±)-**14** and is available free of charge from The Cambridge Crystallographic Data Centre via www.ccdc.cam.ac.uk/data_request/cif.
(8) Ley, S. V.; Norman, J.; William, G. P.; Marsden, S. P. *Synthesis* **1994**, 639–666.

Scheme 3. Construction of Aldehyde Carbonates (−)-**21** and (−)-**22** and Results of Their SmI_2-Induced Cyclizations[a]

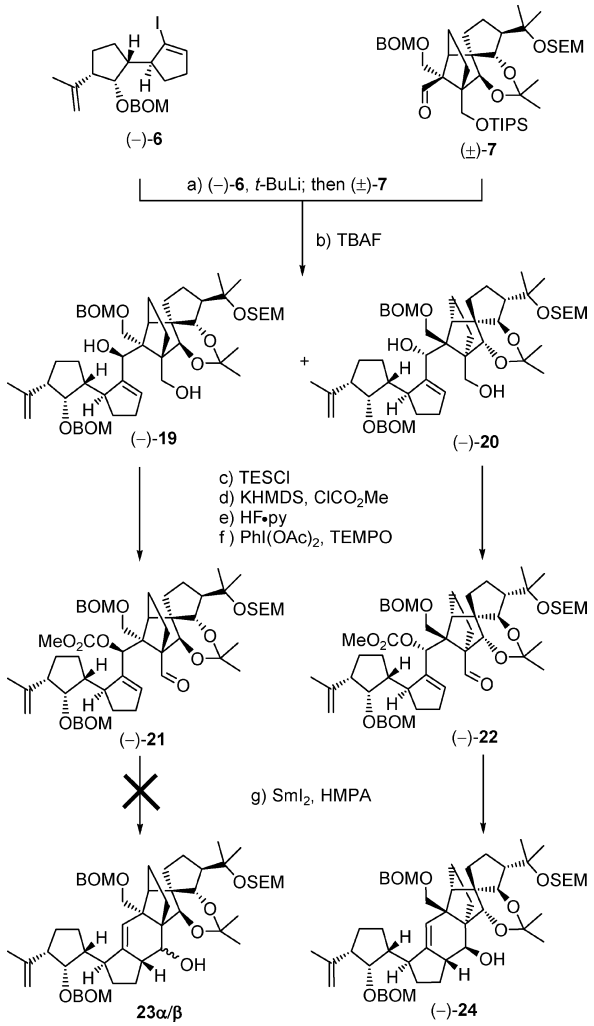

[a] Reagents and conditions: (a) (−)-**6** (1.3 equiv), *t*-BuLi (2.6 equiv), THF, −78 → − 40 °C, 30 min; then (±)-**7** (1.0 equiv), −40 → 0 °C, 20 min; (b) TBAF (3.0 equiv) THF, 25 °C, 2 h, (−)-**19**: 35%, (−)-**20**: 30%; (c) TESCl (2.0 equiv), imidazole (6.0 equiv), CH_2Cl_2, 25 °C, 1 h; (d) KHMDS (0.5 M in toluene, 2.5 equiv), $ClCO_2Me$ (5.0 equiv), Et_3N (6.0 equiv), THF, −78 → 25 °C, 1 h; (e) HF•py/py (1:4), 0 → 25 °C, 12 h, 90% yield for the (−)-**19** route, 87% for the (−)-**20** route; (f) $PhI(OAc)_2$ (2.0 equiv), TEMPO (1.0 equiv), CH_2Cl_2, 25 °C, 24 h, (−)-**21**: 87%, (−)-**22**: 97%; (g) SmI_2 (0.1 M in THF, 5.0 equiv), HMPA (15 equiv), THF, −10 → 25 °C, 30 min, (−)-**24**: 76%.

Scheme 4. Construction of Tri-SEM Protected Aldehyde (±)-**27** and Its Elaboration to Hydroxy Olefins (−)-**31** and (−)-**32**[a]

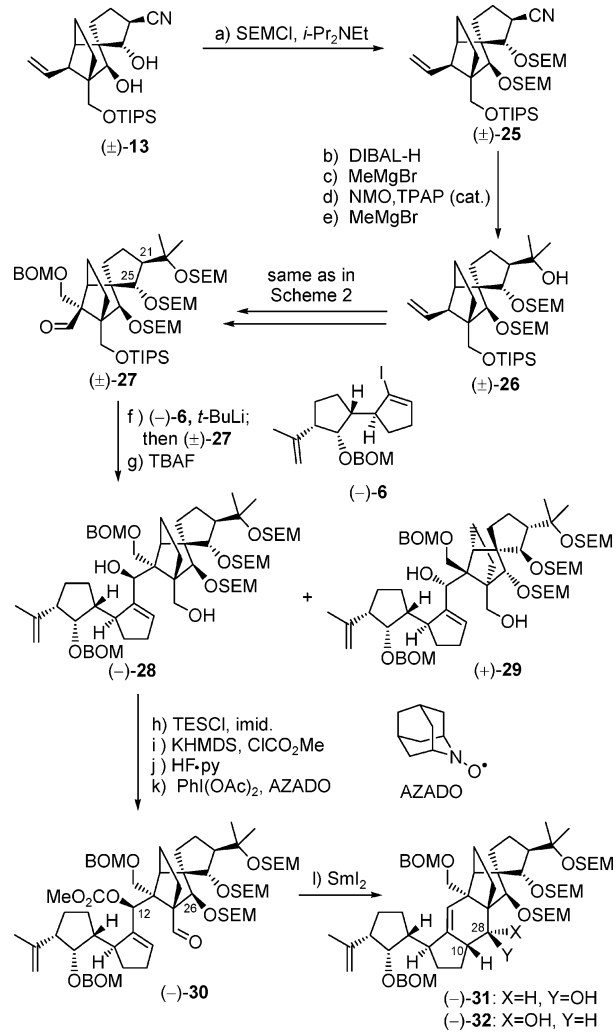

[a] Reagents and conditions: (a) SEMCl (10 equiv), *i*-Pr_2NEt (30 equiv), CH_2Cl_2, 50 °C, 48 h, 90%; (b) DIBAL-H (1.1 equiv), toluene, −78 → 30 °C, 1 h; then 0.1 N aq HCl, 25 °C, 20 min; (c) MeMgBr (10 equiv), THF, 0 °C, 30 min; (d) NMO (2.0 equiv), TPAP (0.05 equiv), CH_2Cl_2/MeCN (7:1), 25 °C, 3 h; (e) MeMgBr (10 equiv), THF, −10 °C, 20 min, 72% for the four steps; (f) (−)-**6** (1.3 equiv), *t*-BuLi (2.6 equiv), THF, −78 → −40 °C, 30 min; then (±)-**27** (1.0 equiv), −40 → 0 °C, 20 min; (g) TBAF (3.0 equiv) THF, 25 °C, 6 h, (−)-**28**: 41%, (+)-**29**: 42%; (h) TESCl (2.0 equiv), imidazole (10 equiv), CH_2Cl_2, 25 °C, 5 h; (i) KHMDS (0.5 M in toluene, 5.0 equiv), $ClCO_2Me$ (10 equiv), Et_3N (10 equiv), THF, −78 → 25 °C, 1 h; (j) HF•py/py (1:4), 0 → 25 °C, 36 h, 79% for the three steps; (k) $PhI(OAc)_2$ (2.0 equiv), AZADO (0.1 equiv), CH_2Cl_2, 25 °C, 24 h, 95%; (l) SmI_2 (0.1 M in THF, 4.0 equiv), HMPA (12 equiv), THF, −20 → 25 °C, 3.5 h, (−)-**31**, 33% yield, (−)-**32**, 21%.

originally assigned structure of vannusal B.[1] This plan dictated the installment of a SEM moiety a C_{26} of the cyclization precursor as a facilitating group for the desired ring closure.[1,3] Since the C_{21}/C_{25} *trans* relationship of the substituents precluded the use of the acetonide group as a means to engage these positions, we chose the tri-SEM aldehyde (±)-**27** (see Scheme 4) as the subtarget "northeastern" fragment for our next attempt to construct the desired skeletal framework of vannusal B. The synthesis of this substrate commenced from dihydroxy nitrile (±)-**13** and proceeded along the path shown in Scheme 4. Thus, SEM protection of (±)-**13** (SEMCl, *i*-Pr_2NEt, *n*-Bu_4NI, 90% yield) afforded bis-SEM ether nitrile (±)-**25**, whose conversion to bis-SEM tertiary alcohol (±)-**26** proceeded through the standard sequence of reduction (DIBAL-H)/methylation (MeMgBr)/oxidation (NMO, TPAP cat.)[8]/methylation (MeMgBr) as summarized in Scheme 4 and discussed earlier in connection with the synthesis of (±)-**15** from (±)-**14** (Scheme 2). The rest of the chemistry to aldehyde (±)-**27** and coupling products (−)-**28** and (+)-**29** followed similar lines and proceeded through analogous intermediates as shown in Schemes 2 and 3 (see Scheme 4 for details and yields). The desired diastereoisomer from the two coupling products, intermediate (−)-**28** (perceived to be the correct isomer), was then taken forward to the targeted cyclization substrate aldehyde carbonate (−)-**30** through the previously developed four-step sequence [temporary TES monoprotection, carbonate formation, selective desilylation, and oxidation, this time employing the newly reported AZADO[9] system instead of TEMPO as a catalyst] as summarized in Scheme 4.

The completion of the synthesis of precursor (−)-**30** set the stage for the much anticipated radical/anion-mediated cyclization, intended to forge the elusive skeleton of our targeted molecule. Pleasantly, the C_{26}—SEM group proved cooperative in this instance, facilitating the desired ring closure (SmI_2, HMPA, THF, −20 → 25 °C) to afford a mixture of diastereomeric products (at C_{28}) which were chromatographically separated [(−)-**31**, 33% yield, and (−)-**32**, 21% yield]. As demonstrated previously in the case of the originally assigned structure of vannusal B,[1,3] both diastereoisomers could be processed through separate pathways, to the same diene intermediate, as a prelude to installing the proper configurations at C_{10} and C_{28} (see Scheme 5). Thus, treatment of the diastereomer possessing the *anti* C_{10}/C_{28} H/OH stereochemical relationship [(−)-**32**] with $POCl_3$ in pyridine at 60 °C caused dehydration, furnishing conjugated diene (+)-**34** in 72% yield, while conversion of the *syn* H/OH diastereomer [(−)-**31**] to the same diene required initial formation of the corresponding xanthate [(−)-**33**, NaH, CS_2; MeI] followed by Chugaev elimination[10] (microwave heating, 185 °C, 86% yield for the two steps). Conjugated diene (+)-**34** was converted to the desired alcohol (−)-**35**, possessing the correct C_{10}/C_{28} configuration through a sequence involving hydroboration (first with $ThexBH_2$ and then with BH_3·THF), followed by oxidation (H_2O_2, aq NaOH), to afford the corresponding diol (mixture of diastereomers at C_2, single diastereomer at C_{10} and C_{28}), selective aryl selenation at the primary OH-bearing position (*o*-$NO_2C_6H_4SeCN$, *n*-Bu_3P), and oxidation (H_2O_2, *syn*-elimination of the corresponding aryl selenoxide, 68% overall yield).[11]

Having installed all stereocenters in their desired configuration in structure (−)-**35**, the conversion of the latter compound to the targeted vannusal B structure (+)-**3** proceeded smoothly and in high overall yield as shown in Scheme 5. Thus, the free hydroxyl group of (+)-**35** was first protected, as its TES ether (TESCl, KHMDS, Et_3N, 89% yield) and the BOM groups were removed (LiDBB), to reveal the corresponding diol (−)-**36**, whose primary hydroxyl group was selectively oxidized to the corresponding aldehyde with $PhI(OAc)_2$ and 1-Me-AZADO (cat.),[9] leaving the secondary alcohol exposed to the obligatory acetylation (Ac_2O, Et_3N, 4-DMAP, 87% yield for the two steps) to afford the protected vannusal B structure (+)-**37**. Finally, global desilylation through the action of aq HF in THF led to structure (+)-**3** [C_{21}-*epi*-**2**] in 77% yield.

For the sake of completeness, we also processed intermediate (−)-**24**, possessing the opposite relative stereochemistry of the two domains of the molecule (obtained as discussed above, Scheme 3). Scheme 6 summarizes the sequence employed for the conversion of (−)-**24** to the corresponding vannusal B structure (+)-**d-3** [C_{21}-*epi*-**d-2**], which was considerably shorter than the one used to convert its counterparts [(−)-**31**/(−)-**32**)] to vannusal B structure (+)-**3** due to the fact that the configurations at C_{10} and C_{28} did not require inversion. The sequence began with temporary engagement of the free hydroxyl group within (−)-**24** (TESCl, imid., 83% yield), followed by removal of the BOM group (LiDBB, 84% yield), to afford diol (+)-**38**. Intermediate (+)-**39** was then prepared from the latter compound through selective oxidation of the primary alcohol [$PhI(OAc)_2$, TEMPO, 77% yield], acetylation of the secondary alcohol (Ac_2O, 4-DMAP, Et_3N), and desilylation (HF·py, THF, 94% for the two steps). Finally, exposure of (+)-**39** to aq HCl caused acetonide cleavage to afford targeted vannusal B structure (+)-**d-3** [C_{21}-*epi*-**d-2**].

The spectroscopic data of synthetic vannusal B structure (+)-**3** were consistent with its structure, but again, disappointingly, did not match those of natural vannusal B,[2] and neither did those

Scheme 5. Total Synthesis of Vannusal B Structure (+)-**3** [C_{21}-*epi*-**2**][a]

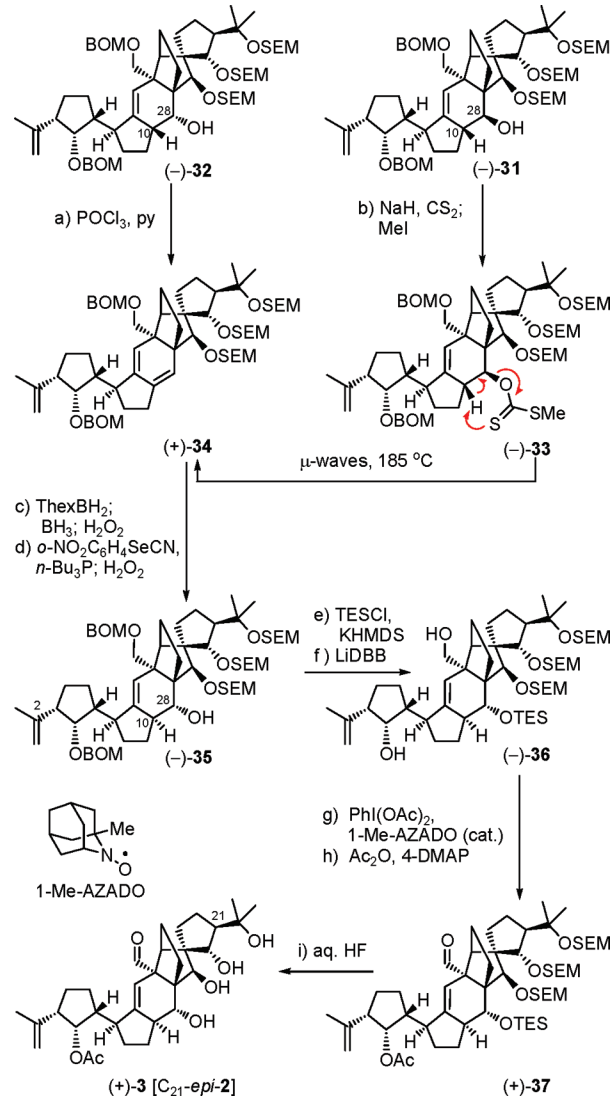

[a] Reagents and conditions: (a) $POCl_3$, py, 60 °C, 1 h, 72% (b) NaH (15 equiv), CS_2 (30 equiv), THF, 0 → 25 °C, 30 min; then MeI (45 equiv), 25 °C, 24 h; then 185 °C (μ-waves), *o*-dichlorobenzene, 15 min, 86% for the two steps; (c) $ThexBH_2$ (5.0 equiv), THF, −10 → 25 °C, 0.5 h; then BH_3·THF (15 equiv), 25 °C, 1 h; then 30% H_2O_2/3 N aq NaOH (1:1), 0 → 45 °C, 1 h; 70%; (d) *o*-$NO_2C_6H_4SeCN$ (3.0 equiv), *n*-Bu_3P (9.0 equiv), py (12 equiv), THF, 25 °C; then 30% H_2O_2, 0 → 45 °C, 68%; (e) KHMDS (6.0 equiv), TESCl (4.0 equiv), Et_3N (8.0 equiv), THF, −50 → 25 °C, 30 min, 89%; (f) LiDBB (excess), THF, −78 → −50 °C, 1 h, 83%; (g) $PhI(OAc)_2$ (2.0 equiv), 1-Me-AZADO (0.2 equiv), CH_2Cl_2, 25 °C, 22 h; (h) Ac_2O (30 equiv), Et_3N (90 equiv), 4-DMAP (2.0 equiv), CH_2Cl_2, 25 °C, 36 h, 87% for the two steps; (i) 48% aq HF/THF (1:3), 25 °C, 7 h, 77%.

(9) Shibuya, M.; Tomizawa, M.; Suzuki, I.; Iwabuchi, Y. *J. Am. Chem. Soc.* **2006**, *128*, 84128413. We thank Professor Iwabuchi and Nissan Chemical Industries, Ltd., for generous gifts of AZADO and 1-Me-AZADO catalysts.

(10) Chugaev, L. *Chem. Ber.* **1899**, *32*, 3332–3335. For examples of the Chugaev elimination (xanthate pyrolysis) used in organic synthesis, see: (a) Meulemans, T. M.; Stork, G. A.; Macaev, F. Z.; Jansen, B. J. M.; de Groot, A. J. *J. Org. Chem.* **1999**, *64*, 9178–9188. (b) Nakagawa, H.; Sugahara, T.; Ogasawara, K. *Tetrahedron Lett.* **2001**, *42*, 4523–4526. (c) Padwa, A.; Zhang, H. *J. Org. Chem.* **2007**, *72*, 2570–2582.

(11) Grieco, P. A.; Nishizawa, M. J. *J. Org. Chem.* **1977**, *42*, 1717–1720.

Scheme 6. Total Synthesis of Vannusal B Structure (+)-**d-3** [C_{21}-*epi*-**d-2**][a]

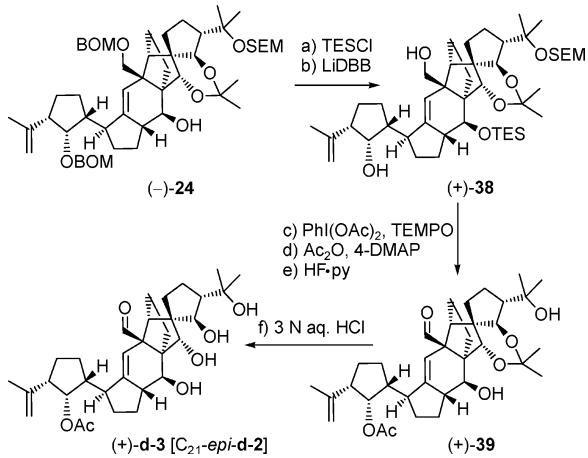

[a] Reagents and conditions: (a) TESCl (2.0 equiv), imidazole (10 equiv) CH_2Cl_2, 3 h, 83%; (b) LiDBB (excess), THF, −78 → −50 °C, 30 min, 84%; (c) $PhI(OAc)_2$ (10 equiv), TEMPO (2.0 equiv), CH_2Cl_2, 25 °C, 24 h, 77%; (d) Ac_2O (40 equiv), Et_3N (40 equiv), 4-DMAP (2.0 equiv), CH_2Cl_2, 25 °C, 12 h; (e) HF•py/THF (1:4), 25 °C, 30 min, 94% for the two steps; (f) 3 N aq HCl/THF (1:3), 25 °C, 12 h, 88% after two cycles.

of its congener (+)-**d-3**, a fact that, at the time, was not surprising given our fixation on the originally assigned relative configuration between the two domains of the vannusal molecule. Despite being disappointing, the spectral comparisons between synthetic vannusal structure (+)-**3** and natural vannusal B were path pointing. A cursory inspection of the diagnostic region (δ 5.7−3.5 ppm) of the ^{1}H NMR spectra of synthetic vannusal B structure (+)-**3** and natural vannusal B (see Figure 8) was sufficient to spot their significant differences. These were the chemical shifts for H_{26} [red, δ = 3.96 ppm for natural vannusal B vs δ = 4.42 ppm for (+)-**3**, $\Delta\delta$ = 0.473 ppm] and H_{25} [blue, δ = 4.37 ppm for natural vannusal B vs δ = 3.96 ppm for (+)-**3**, $\Delta\delta$ = 0.41 ppm] and the distinctly different coupling constant between H_{21} and H_{25} [$JH_{21,25}$ = 2.0 Hz for natural vannusal B vs 8.5 Hz for (+)-**3**]. Panels a and b of Figure 9 respectively depict the ^{1}H and ^{13}C NMR chemical shift differences ($\Delta\delta$, ppm) for each proton and carbon of synthetic vannusal B structure (+)-**3** (red) and its congener (+)-**d-3** (blue) and natural vannusal B (set to zero). In comparing these graphs with those corresponding to the originally assigned structure [(+)-**2**] and its congener (+)-**d-2** (panels a and b of Figure 4), it became clear that the spectral differences between synthetic (+)-**3** and natural vannusal B (set to zero) remained substantial, and for certain signals were even more dramatic in the C_{21}-*epi* compound than the original structures. Furthermore, the major differences appeared in the "northeastern" region of the molecule and to the "right" side of the C_{15}−C_{16} bridgehead. Interestingly, structure (+)-**d-3** was spectrally closer to the natural vannusal B than our "favored" structure (+)-**3**, an observation whose significance we also failed to recognize at the time, as we had for structures (+)-**2** and (+)-**d-2**. It was also interesting to note at this stage that structure (+)-**d-3** exhibited an identical coupling constant to that exhibited by the natural product between H_{10} and H_{28} ($JH_{10,28}$

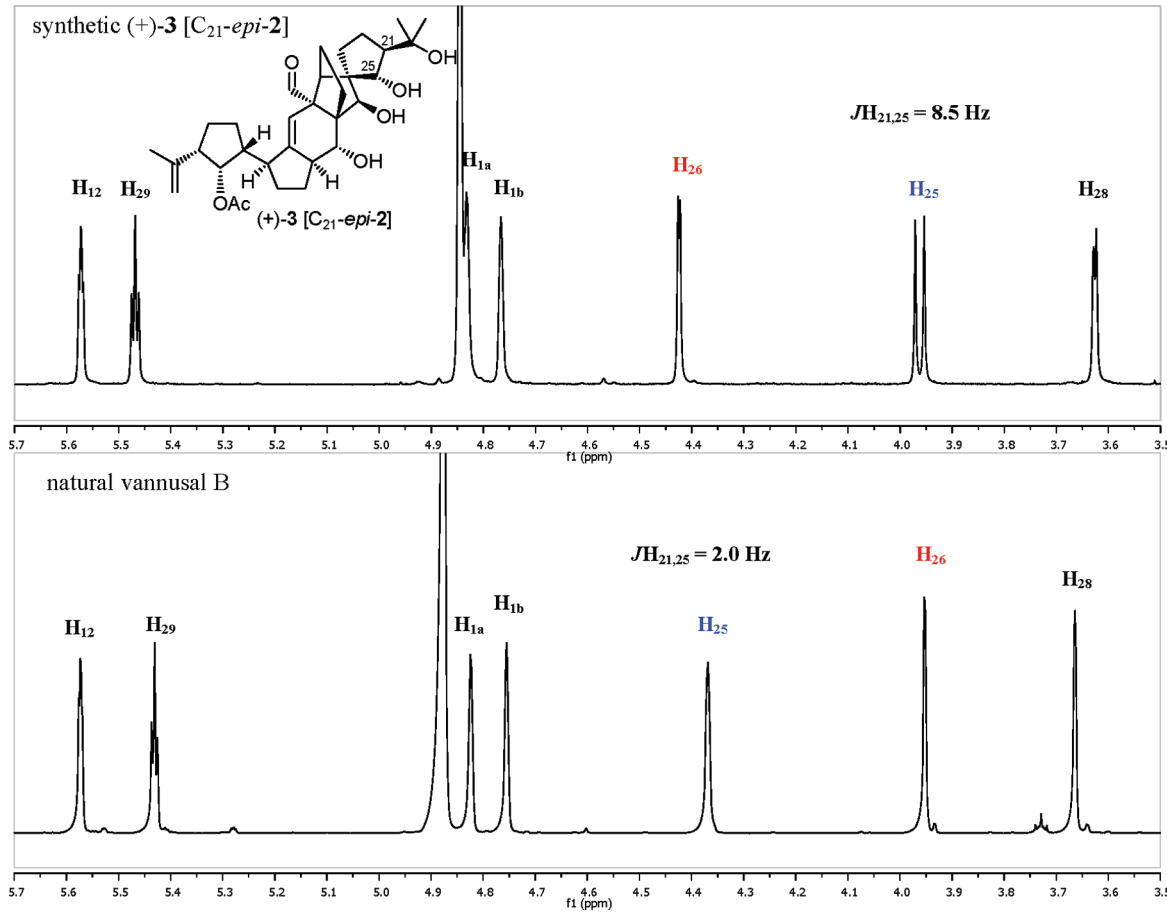

Figure 8. ^{1}H NMR spectral comparison (δ 5.7−3.5 ppm) of synthetic vannusal B structure (+)-**3** (top, d_4-MeOH, 500 MHz) and natural vannusal B (bottom, d_4-MeOH, 600 MHz).

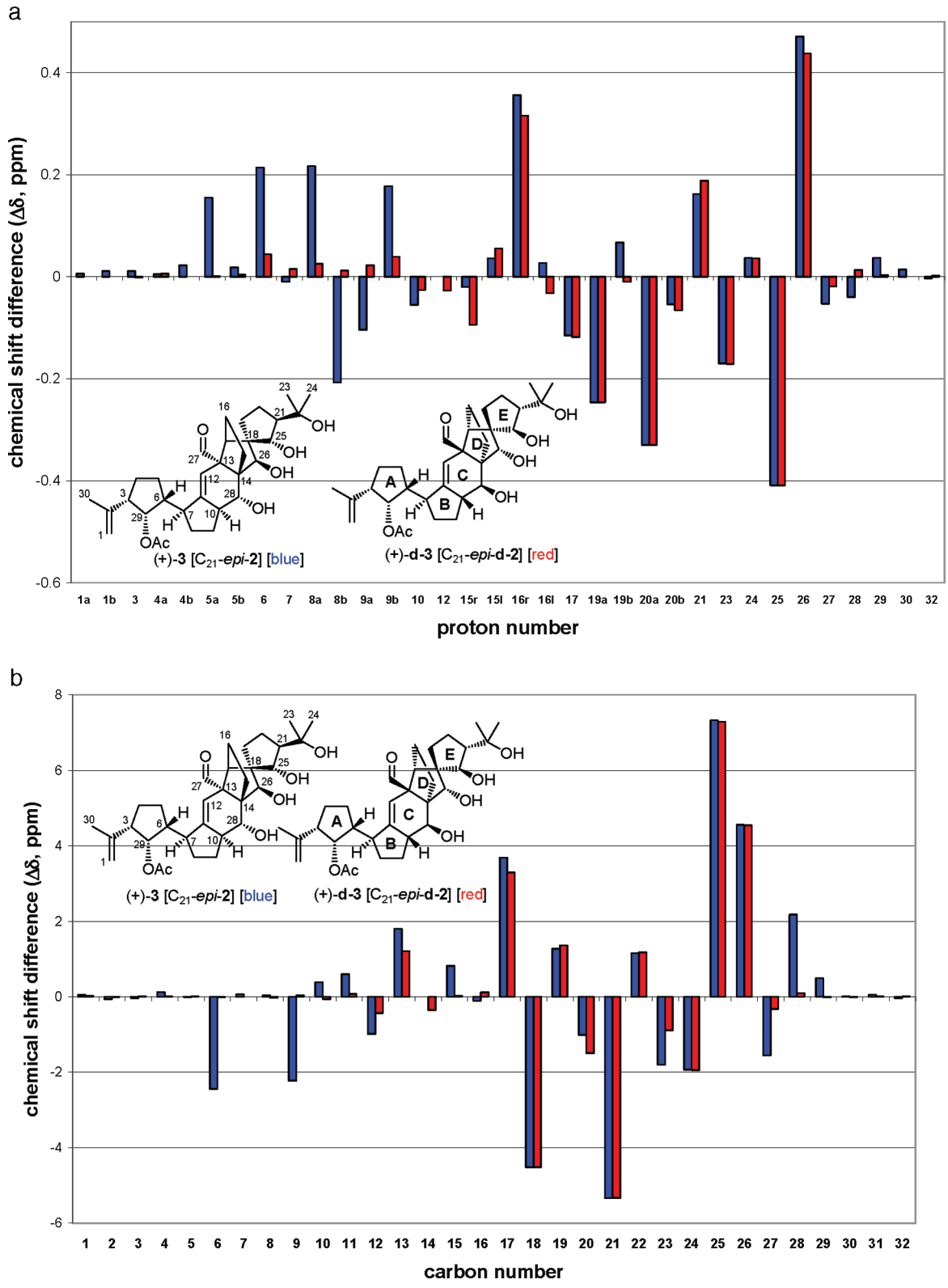

Figure 9. **a.** Graphically depicted ^{1}H chemical shift differences ($\Delta\delta$, ppm) between synthetic vannusal B structures (+)-**3** (blue, d_4-MeOH, 500 MHz) and (+)-**d-3** (red, d_4-MeOH, 600 MHz) and natural vannusal B (600 MHz, set to zero). r = right; l = left. **b.** Graphically depicted ^{13}C chemical shift differences ($\Delta\delta$, ppm) between synthetic vannusal B structures (+)-**3** (blue, 150 MHz) and (+)-**d-3** (red, 150 MHz) and natural vannusal B (set to zero). r = right; l = left.

= 1.8 Hz), whereas our favored congener structure (+)-**3** exhibited a larger coupling constant between these protons ($J_{H10,28}$ = 3.0 Hz). The importance of this observation also went unnoticed at the time, and it was only later that its significance became clear. To be sure, however, we remained convinced that the structural problem was one of stereochemical configuration and that it resided around ring E.

Total Synthesis of Vannusal B Structure (+)-4 [C_{25}-epi, C_{21}-epi-2] and (+)-d-4 [C_{25}-epi, C_{21}-epi-d-2]. With the failure of the spectral properties of (+)-**3** and (+)-**d-3** to match those

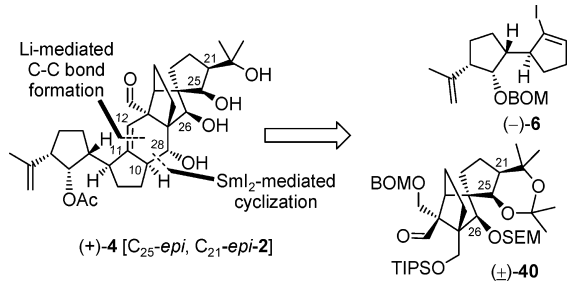

Figure 10. Retrosynthetic analysis of vannusal B structure (+)-**4** [C_{25}-*epi*, C_{21}-*epi*-**2**].

Table 1. Ti- and Li-Mediated Aldol Reactions of Diketone (±)-**41** with Acetone[a]

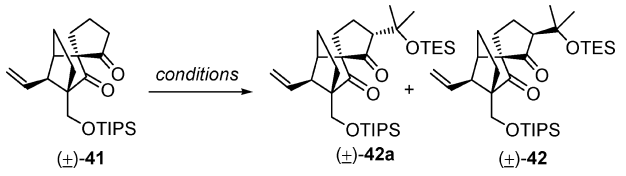

entry	enolate	reagents	temp (°C)	product ratio[b] **42a**:**42**[c]
1	Ti	$TiCl_4$, Et_3N	−40	2:1
2	Ti	$TiCl_4$, Et_3N	−78	6:1
3	Ti	$TiCl_4$, Et_3N	−92	9:1
4	Li	LDA	−78	1:1
5	Li	LDA	−40 to 0	1:3

[a] Reactions were conducted on 0.1−10.0 mmol scale. [b] TESOTf, 2,6-lut. [c] Product ratio determined by ^{1}H NMR spectroscopic analysis.

of natural vannusal B and the intelligence we gathered from the spectroscopic analysis of the synthesized vannusal structures, we proceeded to contemplate and define the next synthetic target of our quest for the true structure of the natural product. The relative coupling constant between H_{25} and H_{21} ($J_{H25,21}$ = 8.5 Hz) exhibited by the *trans* isomer (+)-**3** in comparison to the much smaller value ($J_{H25,21}$ = 2.0 Hz) for the same coupling constant exhibited by natural vannusal B[2] pointed to the remaining E-ring *cis* isomer (+)-**4** (see Figure 10) as the likely structure and so it was that we embarked on the total synthesis of this isomer [and its diastereoisomer (+)-**d-4**, see later, Scheme 10].

According to our developed synthetic strategy toward these targets, aldehyde (±)-**40** was needed in addition to the already available enantiopure vinyl iodide (−)-**6** (see Figure 10). The specific protecting group design within (±)-**40** was based on our previous findings that an OSEM group at C_{26} facilitates the SmI_2-induced ring closure and our expectation that the *syn* relationship of the C_{25}/C_{21} isomer would accommodate an acetonide moiety. The required aldehyde fragment (±)-**40** was constructed as summarized in Scheme 7. Recalling that the opposite *cis* C_{25}/C_{21} isomer of this aldehyde was secured through a route involving a Ti-mediated aldol reaction between diketone (±)-**41** and acetone (see Table 1),[1,3] we sought modified conditions to favor the desired configuration in the aldol product. Table 1 summarizes the results with the titanium (entries 1−3) and lithium (entries 4 and 5) enolates of substrate (±)-**41**. As shown in entry 5, and much to our delight, the lithium enolate of (±)-**41** as generated with LDA (*i*-Pr_2NH, *n*-BuLi in hexanes, THF, −78 → −40 °C) reacted with acetone at −40 → 0 °C to afford the desired C_{21} β-aldol isomer as the major product, which was reacted with TESOTf in the presence of 2,6-lutidine to give TES ether (±)-**42** (66% yield for the two steps), together with its minor C_{21} α-isomer [(±)-**42a**, 21% yield for the two steps]. The diastereoselectivity of this reaction (~3:1) was eroded when it was carried out at −78 °C (Table 1, entry 4) to ~1:1, indicating that, perhaps, it is under thermodynamic control with an equilibrium being established between the two products through retroaldol. Figure 11 provides a postulated mechanistic rationale for the titanium and lithium enolate aldol reactions leading to (±)-**42a** ad (±)-**42**, respectively, as the major products. Thus, we propose the low-temperature (−92 °C) titanium-mediated aldol reaction of **41** to be under kinetic control, with chelation of the titanium enolate to both reacting partners (see **41-TSa** and **41-TSb**) favoring the formation of the C21-α epimer **42a**. In contrast, the LDA-mediated aldol reaction of **41** may be reversible at the higher reaction temperatures employed (−40 → 0 °C). Therefore, a thermodynamic equilibrium between adducts **41-TSc** and **41-TSd** likely

Scheme 7. Construction of Aldehyde (±)-**40**[a]

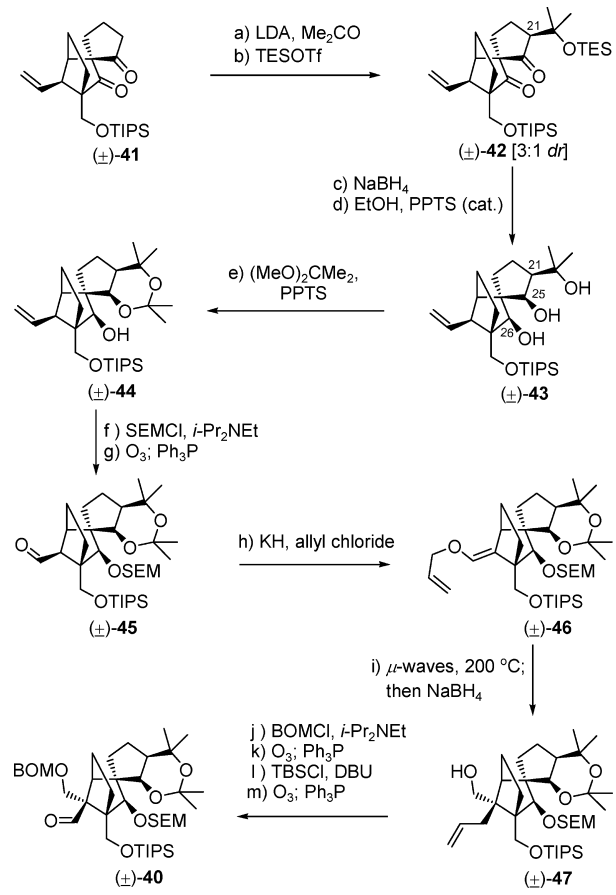

[a] Reagents and conditions: (a) LDA [generated from *i*-Pr_2NH (5.0 equiv), *n*-BuLi (2.5 M in hexanes, 5.0 equiv)], THF, −78 → − 40 °C; then acetone (20 equiv), −40 → 0 °C, 1 h, (3:1 dr); (b) TESOTf (2.0 equiv), 2,6-lutidine (5.0 equiv), −78 → −40 °C, 1 h, 66% for the two steps; (c) $NaBH_4$ (20 equiv), THF/MeOH (1:1), −10 → 25 °C, 4 h; (d) EtOH, PPTS (0.25 equiv), 25 °C, 2 h, 91% for the two steps; (e) $(MeO)_2CMe_2$/DMF (1:1), PPTS (1.0 equiv), 40 °C, 6 h, quant.; (f) SEMCl (5.0 equiv), *i*-Pr_2NEt (15 equiv), *n*-Bu_4NI (1.0 equiv), CH_2Cl_2, 50 °C, 24 h, 97%; (g) O_3, py (1.0 equiv), CH_2Cl_2/MeOH (1:1), −78 °C; then Ph_3P (5.0 equiv), −78 → 25 °C, 1 h, 94%; (h) KH (10 equiv), allyl chloride (20 equiv), HMPA (10 equiv), DME, −10 → 25 °C, 3 h, 88%; (i) *i*-Pr_2NEt (1.0 equiv), *o*-dichlorobenzene, μ-waves, 200 °C, 20 min; then $NaBH_4$ (10 equiv), MeOH, 2 h, 25 °C, 82% for the two steps; (j) BOMCl (3.0 equiv), *i*-Pr_2NEt (10 equiv), *n*-Bu_4NI (1.0 equiv), CH_2Cl_2, 50 °C 12 h; (k) O_3, py (1.0 equiv), CH_2Cl_2/MeOH (1:1), −78 °C; then Ph_3P (5.0 equiv), −78 → 25 °C, 1 h, 94% for the two steps; (l) TBSCl (10 equiv), DBU (20 equiv), CH_2Cl_2, 25 °C, 24 h; (m) O_3, py (1.0 equiv), CH_2Cl_2/MeOH (1:1), −78 °C; then Ph_3P (5.0 equiv), −78 → 25 °C, 1 h, 95% for the two steps.

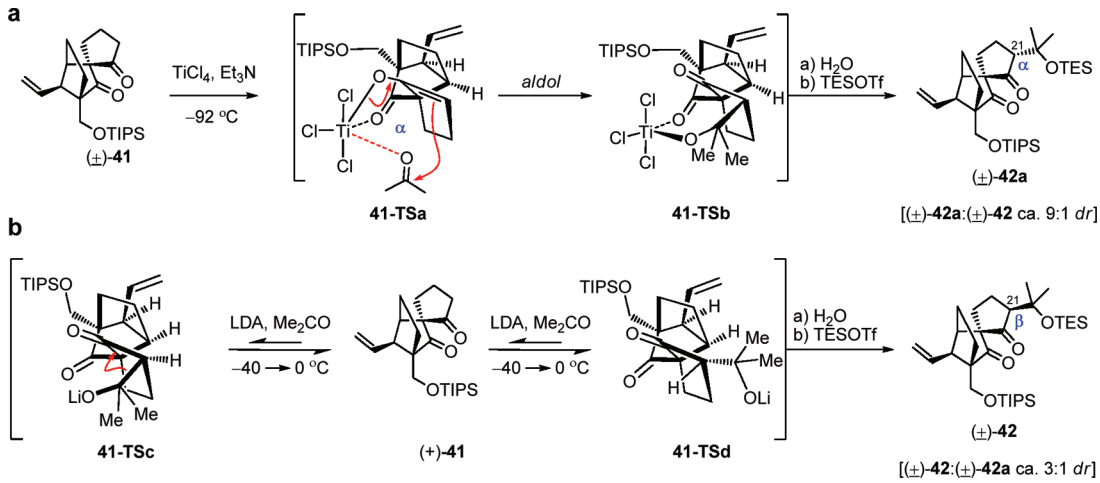

Figure 11. (a) A low-temperature titanium-mediated aldol reaction provides kinetic product (±)-**42a**. (b) A reversible LDA-mediated aldol reaction provides thermodynamic product (±)-**42**.

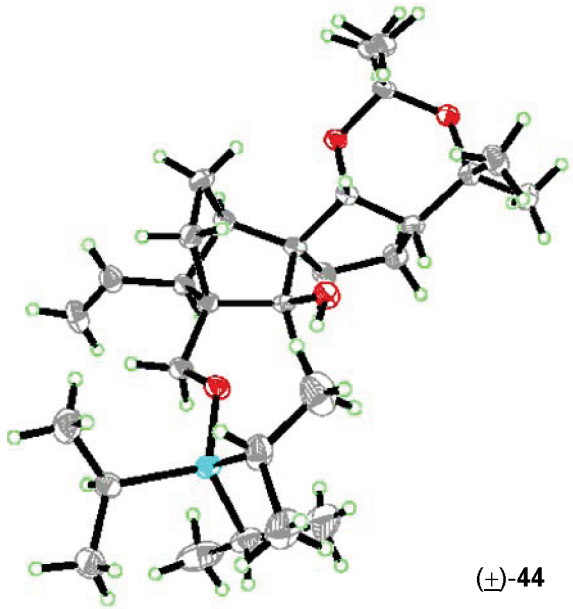

Figure 12. X-ray derived ORTEP of hydroxy acetonide (±)-**44**.

is established, leading to the modest selectivity observed for the C21-β epimer (±)-**42**.

Returning to the construction of the targeted aldehyde (±)-**40** (see Scheme 7), diketone TES ether (±)-**42** was diastereoselectively reduced with $NaBH_4$ in MeOH/THF (1:1) at −10 °C to afford, upon desilylation [EtOH, PPTS (cat.)], triol (±)-**43** in 91% overall yield as a single diastereomer. Treatment of the latter with $(MeO)_2CMe_2$ in the presence of PPTS at ambient temperature led to the isolation of the crystalline hydroxy acetonide (±)-**44** (mp 77−78 °C, EtOAc/hexanes) in quantitative yield. X-ray crystallographic analysis of this compound (see ORTEP, Figure 12)[12] unambiguously confirmed its structure and those of its progenitors [i.e., (±)-**43** and (+)-**42**]. Installment of a SEM group (SEMCl, *i*-Pr_2NEt, *n*-Bu_4NI, 97% yield) at the free hydroxyl group of (±)-**44**, followed by ozonolytic cleavage of its olefinic bond (O_3; Ph_3P, 94% yield), led to aldehyde (±)-**45**, whose conversion to the desired aldehyde fragment [(±)-**40**] followed a similar pathway as previously delineated [through intermediates (±)-**46** and (±)-**47**, see Scheme 7 for details].

With ample quantities of both "southwestern" [(−)-**6**] and "northeastern" [(±)-**40**] fragments in hand, the drive toward the targeted structures (+)-**4** and (+)-**d-4** became feasible (see Scheme 8). Thus, as previously demonstrated, the coupling of enantiopure vinyl iodide (−)-**6** with racemic aldehyde (±)-**40** proceeded smoothly through the lithium derivative of (−)-**6** (*t*-BuLi) to afford, after removal of the TIPS group (TBAF, 25 °C), a mixture of diastereomeric diols (−)-**48** and (−)-**49** (72% combined yield for the two steps, ∼1:1 dr), which were chromatographically separated. Coupling products (−)-**48** and (−)-**49** were individually converted to cyclization precursors (−)-**50** and (+)-**51**, respectively, through the same sequence of reactions as previously described, involving temporary silylation of the primary hydroxyl group (TESCl, imid.), carbonate formation at the secondary position (KHMDS, $ClCO_2Me$), removal of the TES group [HF·py, 84% overall yield from (−)-**48**; 80% overall yield for (−)-**49**], and oxidation of the liberated primary hydroxyl group [$PhI(OAc)_2$, AZADO (cat.),[9] 95% yield for (−)-**50**, 97% yield for (+)-**51**] as summarized in Scheme 8. When aldehyde carbonate (−)-**50** was exposed to the SmI_2—HMPA conditions (−10 → 25 °C), the desired ring closure took place, leading to polycyclic product (−)-**52** in 74% yield as a single diastereoisomer, but possessing the undesired C_{10}/C_{28} configurations in relation to the "northeastern" part of the molecule. However, when its diastereomeric congener (+)-**51** was exposed to the same conditions, hydroxy olefin (+)-**53** was formed in 84% yield and, again, as a single diastereomer, except that this time both newly generated stereocenters (C_{10}/C_{28}) were of the desired relative configuration with regards to the "northeastern" domain.

First to be advanced from this point was hydroxy olefin (−)-**52**, which underwent xanthate formation at C_{28} (NaH, CS_2; MeI) and, upon heating under microwave conditions (185 °C), *syn* elimination to afford conjugated diene (+)-**54** (89% overall yield) as shown in Scheme 9. The latter compound was converted to the desired C_{10}/C_{28} diastereomer hydroxy olefin (−)-**55** through the previously developed sequence involving hydroboration/oxidation (ThexBH$_2$; BH_3·THF; H_2O_2/NaOH, 70% overall yield) and arylselenylation/*syn* elimination (*o*-$NO_2C_6H_4SeCN$, *n*-Bu_3P; H_2O_2, 70% overall yield).[11] Intermedi-

(12) CCDC-757085 contains the supplementary crystallographic data for hydroxy acetonide (±)-**44**. This data can be obtained free of charge from the Cambridge Crystallographic Data Centre via www.ccdc.cam.ac.uk/data_request/cif.

Scheme 8. Construction of Hydroxy Olefins (−)-**52** and (+)-**53**[a]

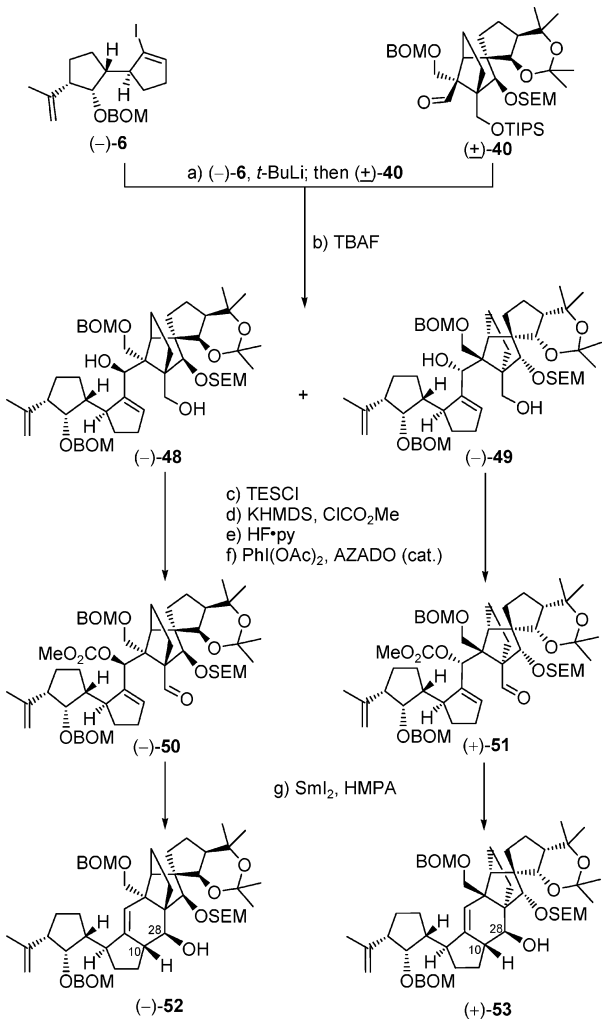

[a] Reagents and conditions: (a) (−)-**6** (1.3 equiv), *t*-BuLi (2.6 equiv), THF, −78 → −40 °C, 30 min; then (±)-**40** (1.0 equiv), −40 → 0 °C, 20 min; (b) TBAF (4.0 equiv) THF, 25 °C, 30 min, (−)-**48**: 36%, (−)-**49**: 36%. (c) TESCl (2.0 equiv), imidazole (4.0 equiv), CH_2Cl_2, 25 °C, 30 min; (d) KHMDS (0.5 M in toluene, 2.5 equiv), $ClCO_2Me$ (3.0 equiv), Et_3N (3.0 equiv), THF, −78 → 25 °C, 1 h; (e) HF•py/py (1:4), 0 → 25 °C, 12 h; (f) $PhI(OAc)_2$ (3.0 equiv), AZADO (0.1 equiv), CH_2Cl_2, 25 °C, 24 h, (−)-**50**: 80% for the four steps, (+)-**51**: 78% for the four steps; (g) SmI_2 (0.1 M in THF, 5.0 equiv), HMPA (15 equiv), THF, −10 → 25 °C, 30 min, (−)-**52**: 74%, (+)-**53**: 84%.

ate (−)-**55** was then transformed to diol (+)-**56** through sequential silylation (KHMDS, TESCl, 94% yield) and cleavage of the BOM groups (LiDBB, 82% yield). The final three steps to structure (+)-**4**, involving sequential oxidation of the primary hydroxyl group within (−)-**55** [$PhI(OAc)_2$, TEMPO, 92% yield], acetylation of the secondary hydroxyl group (Ac_2O, Et_3N, 4-DMAP, quant.), and global deprotection (aq HF, 75% yield), proceeded smoothly as it had previously. However, and again much to our chagrin, the ^1H and ^{13}C NMR spectra of synthetic (+)-**4** did not match those of the natural product.

The conversion of the other diastereomeric polycycle intermediate (+)-**53** to diastereomeric vannusal B structure (+)-**d-4** is summarized in Scheme 10. Thus, following the previously developed short sequence, involving silylation (KHMDS, TESCl) and cleavage of the BOM groups (LiDBB) to afford diol (+)-**58** (77% for the two steps), sequential oxidation of the primary hydroxyl group within the latter compound [$PhI(OAc)_2$, TEMPO, 85% yield], and acetylation of the secondary hydroxyl group (Ac_2O, Et_3N, 4-DMAP, quant.), furnished precursor (+)-**59**, whose global desilylation (aq HF, 77% yield) proceeded smoothly to unveil vannusal B structure (+)-**d-4**.

Scheme 9. Total Synthesis of Vannusal B Structure (+)-**4** [C_{25}-*epi*, C_{21}-*epi*-**2**][a]

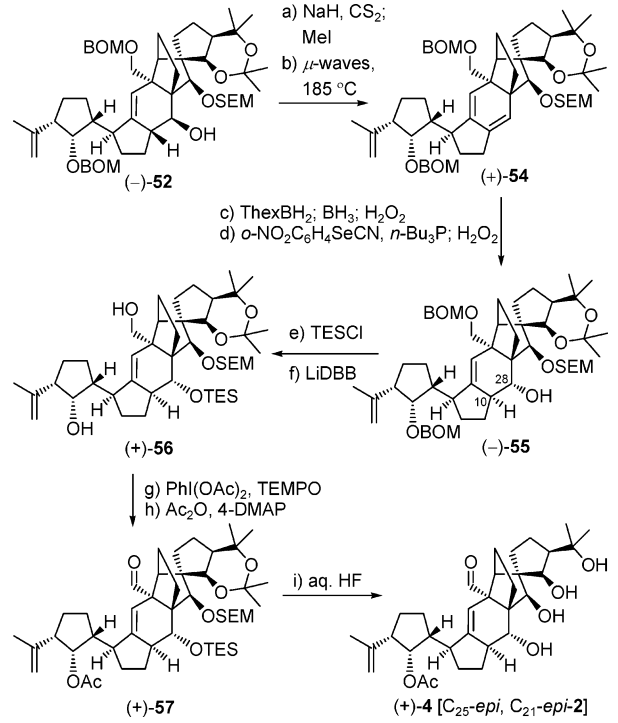

[a] Reagents and conditions: (a) NaH (8.0 equiv), CS_2 (8.0 equiv), THF, 0 → 25 °C, 20 min; then MeI (12 equiv), 25 °C, 24 h; (b) μ-waves, 185 °C, *o*-dichlorobenzene, 15 min, 89% for the two steps; (c) $ThexBH_2$ (5.0 equiv), THF, −10 → 25 °C, 0.5 h; then BH_3•THF (15 equiv), 25 °C, 1 h; then 30% H_2O_2/3 N aq NaOH (1:1), 0 → 45 °C, 1 h; 70%; (d) o-$NO_2C_6H_4SeCN$ (3.0 equiv), n-Bu_3P (9.0 equiv), py (12 equiv), THF, 25 °C; then 30% H_2O_2, 0 → 45 °C, 70%; (e) KHMDS (6.0 equiv), TESCl (4.0 equiv), Et_3N (8.0 equiv), THF, −50 → 25 °C, 30 min, 94%; (f) LiDBB (excess), THF, −78 → −50 °C, 1 h, 82%; (g) $PhI(OAc)_2$ (3.0 equiv), TEMPO (1.0 equiv), CH_2Cl_2, 25 °C, 24 h, 92%; (h) Ac_2O (30 equiv), Et_3N (90 equiv), 4-DMAP (1.0 equiv), CH_2Cl_2, 25 °C, 12 h, quant.; (i) 48% aq HF/THF (1:3), 25 °C, 7 h, 75%.

Scheme 10. Total Synthesis of Vannusal B Structure (+)-**d-4** [C_{25}-*epi*, C_{21}-*epi*-**d-2**][a]

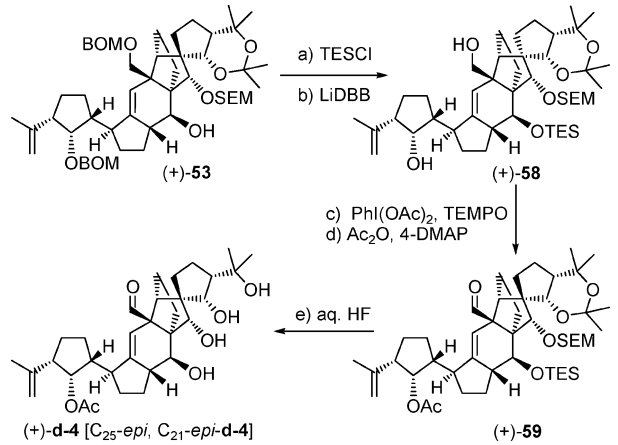

[a] Reagents and conditions: (a) KHMDS (0.5 M toluene, 4.0 equiv), TESCl (8.0 equiv), Et_3N (10 equiv), THF, 20 min; (b) LiDBB (excess), THF, −78 → −50 °C, 30 min, 77% for the two steps; (c) $PhI(OAc)_2$ (2.0 equiv), TEMPO (1.0 equiv), CH_2Cl_2, 25 °C, 48 h; (d) Ac_2O (20 equiv), Et_3N (30 equiv), 4-DMAP (1.0 equiv), CH_2Cl_2, 25 °C, 12 h, 85% for the two steps; (e) aq HF/THF (1:3), 25 °C, 7 h, 77%.

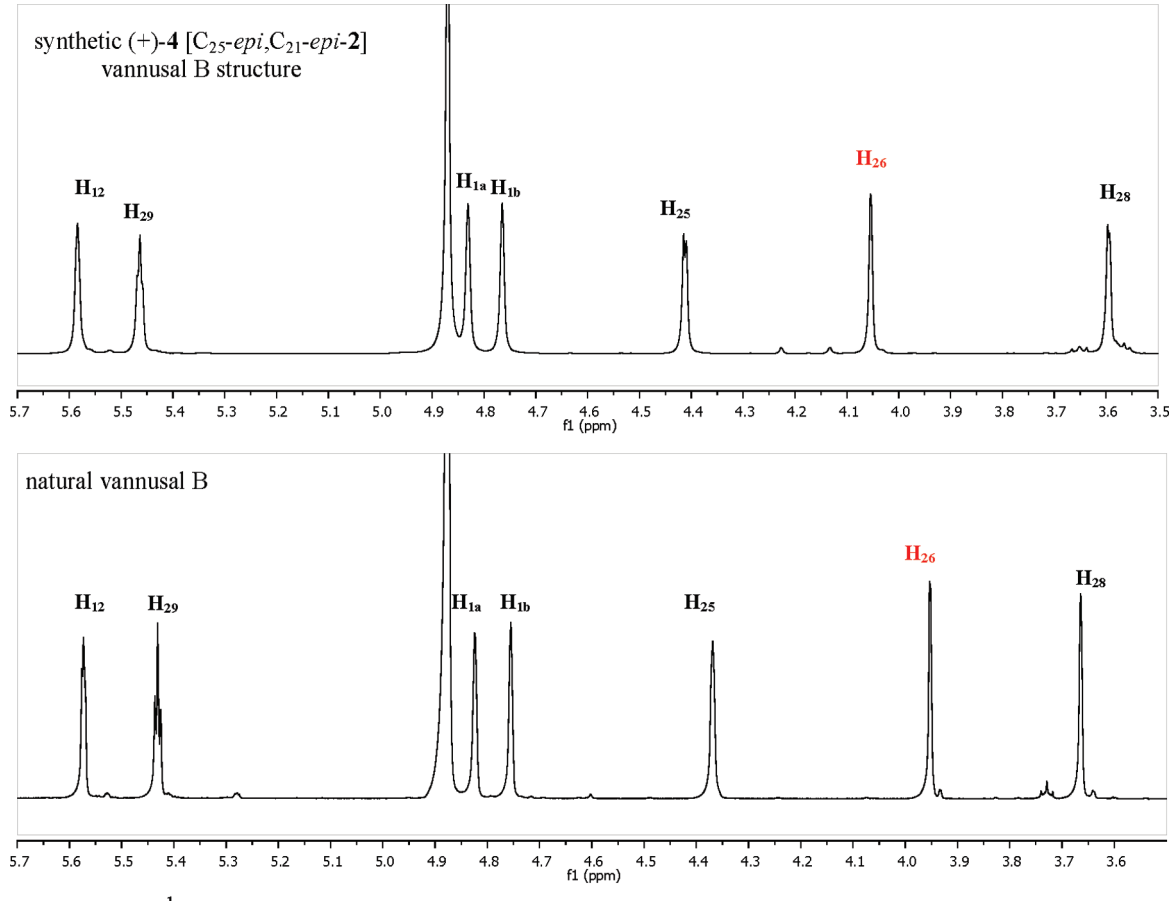

Figure 13. ^{1}H NMR spectral comparison (δ 5.7−3.5 ppm, d_4-MeOH, 600 MHz) of synthetic vannusal B structure (+)-**4** (top) and natural vannusal B (bottom).

In examining the diagnostic regions of synthetic vannusal B structure (+)-**4** and natural vannusal B (see Figure 13), we noticed with interest some striking similarities between them as opposed to our previous comparisons. For the first time in our search for the right structure, the corresponding H_{25}, H_{26}, and H_{28} signals for the two, still nonidentical structures converge to close proximity with each other. Most encouraging was the $\Delta\delta$ ~0.1 ppm shift of the H_{26} signal of (+)-**4** (δ 4.054 ppm) which, until then, had remained relatively downfield (e.g., **2**: δ 4.438 ppm; **3**: δ 4.424 ppm) from the position of the corresponding signal of the natural product (δ = 3.953 ppm). Furthermore, we were pleased to see the restoration of a relatively small coupling constant between H_{25} and H_{21} ($JH_{25,21}$ = 3.0 Hz) in structure (+)-**4**, suggesting that we were on the right track with the *cis* C_{25}/C_{21} stereorelationship.

A more thorough comparison of the ^{1}H and ^{13}C NMR chemical shift differences between (+)-**4** (blue) and (+)-**d-4** (red) with natural vannusal B (set to zero) is graphically depicted in panels a and b, respectively, of Figure 14. Among the many discrepancies, the most striking difference centered on C_{21} [^{1}H $\Delta\delta$ +0.295 ppm, Figure 14a; ^{13}C $\Delta\delta$ −10.73 ppm, Figure 14b]. Additionally, we began noticing a curious trend in the incongruity of the left-half fragment (A/B-ring domain; C_1-C_{12}) of our diastereomers thus far prepared as compared to the natural product.[2] The recognition of the persistent NMR spectroscopic discrepancies in the "southwestern" region, despite the positive response of the structural adjustments in the "northeastern" site of the molecule in terms of chemical shifts (especially in the diagnostic region), led us to wonder whether the initial misassignment to the vannusals was rooted not just in its "northeastern" region, but also in its "southwestern" domain (i.e., A/B ring system).

Model AB Ring System Studies. Having assured ourselves (as it turned out, incorrectly) of the correctness of the "northeastern" domain of the vannusal molecule, we turned our attention to its "southwestern" region. The original configurational assignments around the AB ring system of the vannusals were based on ^{1}H/^{1}H NMR coupling constants (*J*-values; red) and nuclear overhauser effects (NOEs; blue), as summarized in Figure 15, for vannusal A.[2] Specifically, the relatively large coupling constant between H_6 and H_7 ($JH_{6,7}$ = 10.0 Hz) supported the *anti* periplanar relationship between these protons, while the shared, relatively small coupling constant between H_{29} and H_3 and H_6 [$JH_{29,3}$ (eq, ax) = $JH_{29,6}$ (eq, ax) = 3.5 Hz] suggested the *all-cis* relationship of these protons, a conclusion further supported by the NOEs observed between H_3 and H_{29}, and H_{29} and H_6. Interestingly, no NOE between H_3 and H_6 (that would have revealed a true 1,3-diaxial interaction between them) was reported. Additionally, NOEs were observed around the flanks of the A ring (i.e., between H_{29} and $H_{8\beta}$, and $H_{5\alpha}$ and H_{12}, see Figure 15), which led to the placement of its C_3 and C_{29} substituents as shown (*cis*). Finally, an observed NOE between H_7 and H_{10} was the only evidence pointing to the assigned configuration of the important C_7 stereocenter with respect to the "northeastern" domain of the molecule.[2]

Despite this supporting spectroscopic evidence for the originally assigned structure of the AB region of the vannusals, and because of the rather unreliable nature of

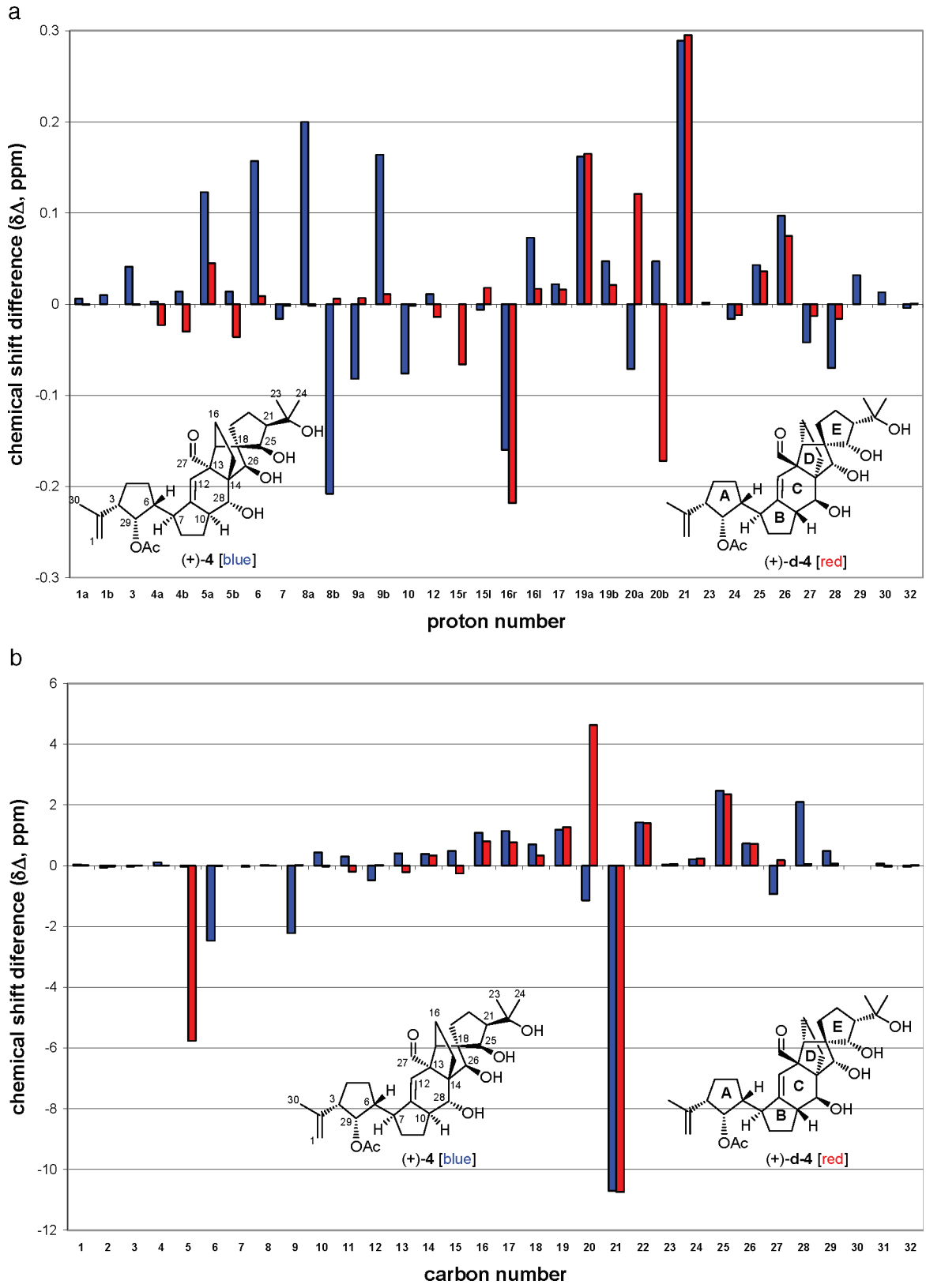

Figure 14. (a) Graphically depicted ^{1}H chemical shift differences ($\Delta\delta$, ppm, d_4-MeOH, 600 MHz) between vannusal B structures (+)-**4** (blue) and (+)-**d-4** (red) and natural vannusal B. r = right; l = left. (b) Graphically depicted ^{13}C chemical shift differences ($\Delta\delta$, ppm, 150 MHz) between synthetic vannusal B structures (+)-**4** (blue) and (+)-**d-4** (red) and natural vannusal B (set to zero).

NMR spectroscopic information for stereochemical assignments around five-membered rings[15] as we had already experienced, we decided to prepare all eight diastereomers of the AB ring system (see Figure 16) and study their NMR spectra in order to derive useful information regarding the true structures of the vannusals. We reasoned that such an investigation could also prove to be useful in solving other stereochemical problems involving five-membered rings

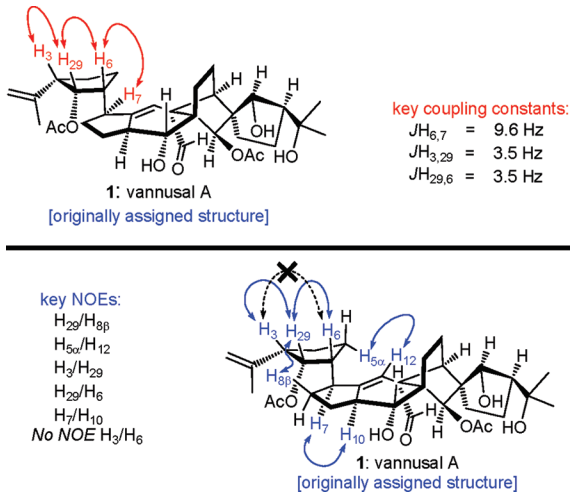

Figure 15. Key $^1H/^1H$ couplings (red, *J*-value) and NOEs (blue) used to assign the original structure of vannusal A.[2]

beyond the vannusals conundrum. The syntheses of model systems **60**−**67** were based, for the most part, on the chemistry developed in our quest for vinyl iodide (−)-**6** discussed previously.[1,3] Schemes 11 and 12 summarize the devised routes to these compounds, starting with epoxides (+)-**68** and **68a/b** and ketone (−)-**74**.

Thus, acetates (+)-**60** and (+)-**61** were prepared (as shown in Scheme 11) from the corresponding alcohols [(+)-**69** and (+)-**70**, respectively, Ac_2O, 4-DMAP, 96% yield], which were obtained from epoxide (+)-**68** as previously described.[1,3] The previously synthesized[1] diastereomeric mixture of epoxides **68a/b** (∼1:1 dr) was converted to alcohols (+)-**71** and (+)-**69** through the action of 2-lithiopropene in the presence of $BF_3 \cdot Et_2O$ in 80% combined yield (∼1:1 dr). Chromatographic separation of the two diastereomers allowed conversion of pure (+)-**71** to acetates (+)-**62** (Ac_2O, 4-DMAP, Et_3N, 92% yield) and (+)-**63** [(i) Ph_3P, *p*-$NO_2C_6H_4CO_2H$, DEAD; (ii) DIBAL-H; (iii) Ac_2O, 4-DMAP, Et_3N, 11% yield for the three steps, unoptimized].

The synthesis of the other four diastereomeric acetates (**64**−**67**) required initial epimerization of the previously synthesized ketone (+)-**73**,[1] an objective that was met by refluxing the latter in benzene in the presence of DBU (Scheme 12). Under these conditions, a favorable equilibrium between the desired epimeric ketone (−)-**74** and the starting C_6 epimer (+)-**73** [(−)-**74**/(−)-**73**, ∼2:1 dr, 98% combined yield] was established. Chromatographic separation of ketone (−)-**74** allowed its further elaboration to olefin (+)-**75** [KHMDS, $PhNTf_2$; Et_3SiH, $Pd(Ph_3P)_4$ (cat.), 91% overall yield]. Epoxidation of the latter with *m*-CPBA resulted in the formation of a mixture of the two epimeric epoxides **76a/b** (86% yield ∼1:1 dr), whose opening with 2-lithiopropene (prepared from 2-bromopropene and *t*-BuLi) in the presence of $BF_3 \cdot Et_2O$ led to diastereomeric alcohols (−)-**77** (22% yield) and (−)-**78** (28% yield), together with recovered starting material **76a/b** (28%). Acetylation of hydroxy

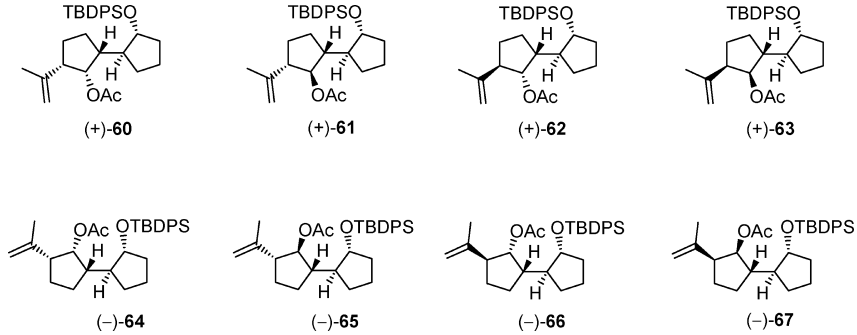

Figure 16. Structures of targeted AB model systems **60**−**67**.

Scheme 11. Construction of Model Compounds (+)-**60**, (+)-**61**, (+)-**62**, and (+)-**63**[a]

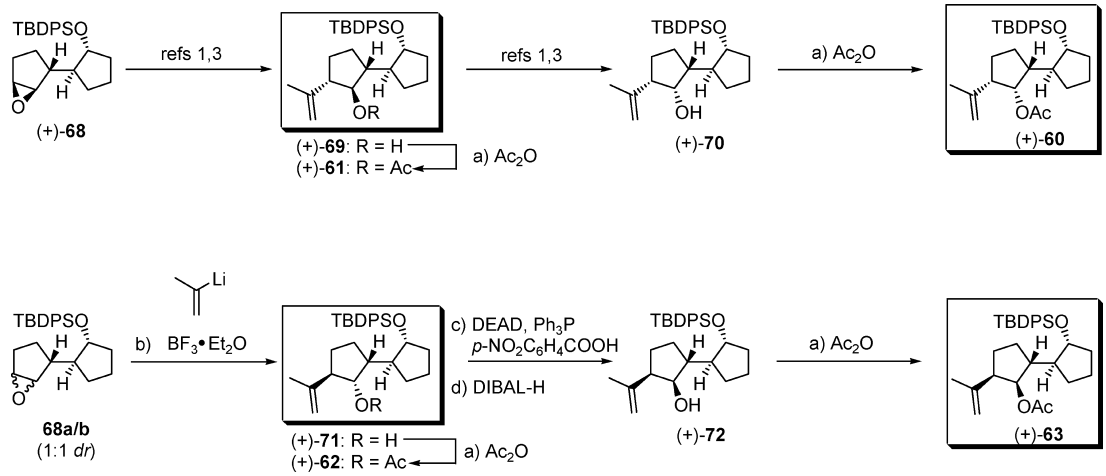

[a] Reagents and conditions: (a) Ac_2O (5.0 equiv), Et_3N (5.0 equiv), 4-DMAP (1.0 equiv), CH_2Cl_2, 0.5−8 h, (+)-**60** (96%), (+)-**61** (96%), (+)-**62** (92%), (+)-**63** [11% overall yield from (+)-**71**, unoptimized]; (b) 2-bromopropene (4.5 equiv), *t*-BuLi (1.7 M in pentane, 8.0 equiv), THF, −78 °C, 5 min; then $BF_3 \cdot Et_2O$ (2.0 equiv), 2 min; then **68a/68b** (∼1:1 dr), −78 → −20 °C, 30 min, 80% [(+)-**69**/(+)-**71** ∼1:1 dr]; (c) *p*-$NO_2C_6H_4CO_2H$ (3.0 equiv), DEAD (3.0 equiv), Ph_3P (3.0 equiv), benzene, 25 °C, 18 h; (d) DIBAL-H (1.0 M in CH_2Cl_2, 2.5 equiv), CH_2Cl_2, −78 °C, 30 min.

Scheme 12. Synthesis of AB Model Systems (−)-**64**, (−)-**65**, (−)-**66**, and (−)-**67**[a]

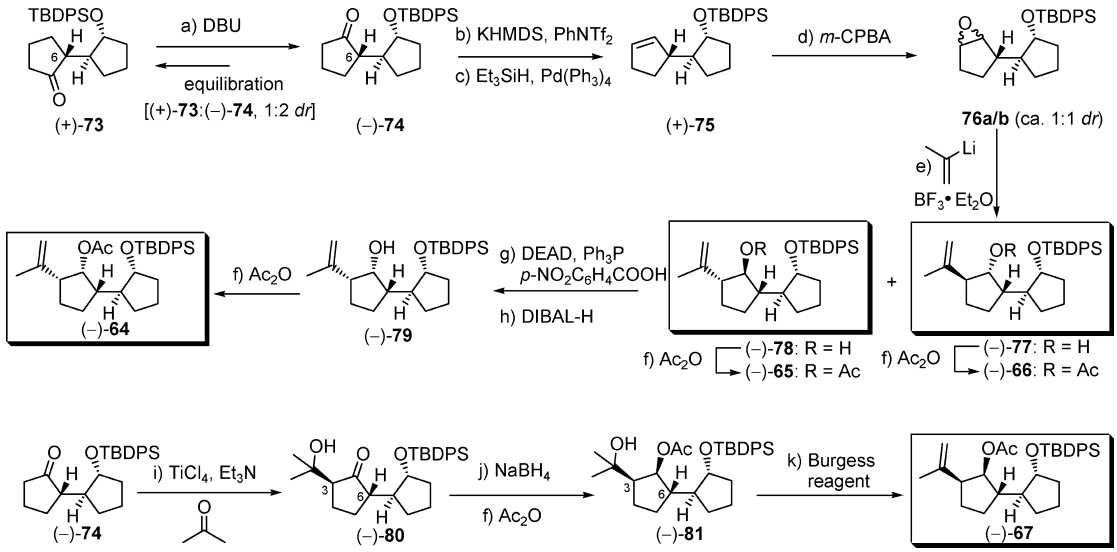

[a] Reagents and conditions: (a) DBU (1.0 equiv), benzene, 90 °C, 12 h, [2:1, (−)-**74**/(+)-**73**, ∼2:1], 98% combined yield, chromatographic separation; (b) KHMDS (0.5 M in toluene, 1.5 equiv), $PhNTf_2$ (1.5 equiv), THF, −78 → −40 °C, 30 min; (c) Et_3SiH (2.0 equiv), $Pd(Ph_3P)_4$ (0.05 equiv), DMF, 50 °C, 3 h, 91% for the two steps; (d) *m*-CPBA (2.0 equiv), CH_2Cl_2, −10 → 25 °C, 12 h, 86% (∼1:1 dr); (e) 2-bromopropene (4.5 equiv), *t*-BuLi (1.7 M in pentane, 8.0 equiv), THF, −78 °C, 5 min; then $BF_3 \cdot Et_2O$ (2.0 equiv), 2 min; then **76a/b**, −78 → −20 °C, 30 min, (−)-**77**: 22% yield, (−)-**78**: 28% yield, recovered starting material (28%); (f) Ac_2O (5.0 equiv), Et_3N (5.0 equiv), 4-DMAP (1.0 equiv), CH_2Cl_2, 25 °C, 4−6 h, (−)-**65** (86%), (−)-**66** (86%), (−)-**64** (94%), (−)-**81** (71% for the two steps); (g) *p*-$NO_2C_6H_4CO_2H$ (1.5 equiv), DEAD (1.5 equiv), Ph_3P (1.8 equiv), benzene, 0 → 25 °C, 18 h, 39%; (h) DIBAL-H (1.0 M in CH_2Cl_2, 2.5 equiv), CH_2Cl_2, −78 °C, 30 min, 81%; (i) $TiCl_4$ (1.2 equiv), Et_3N (3.0 equiv), acetone (20 equiv), CH_2Cl_2, −78 °C, 30 min, 92%; (j) $NaBH_4$ (10 equiv), THF/MeOH (1:1), 0 °C, 1 h (∼6:1 dr), see (f) for yield; (k) Burgess reagent (10 equiv), benzene, 80 °C, 1 h, 50%.

olefin (−)-**78** under standard conditions furnished acetate model system (−)-**66** (86% yield, whereas Mitsunobu inversion ([Ph_3P, *p*-$NO_2C_6H_4CO_2H$, DEAD, 39% yield; DIBAL-H) gave diastereomeric hydroxy olefin (−)-**79**, whose acetylation, as before, led to the desired diastereomeric acetate (−)-**64** (76% yield for the two steps). Similarly, acetylation of alcohol (−)-**77** proceeded smoothly to afford the next diastereomeric acetate [(−)-**66**, 86% yield]. The intended Mitsunobu reaction of this alcohol [(−)-**77**] as the shortest route to acetate (−)-**67** proved unsuccessful, presumably due to severe steric hindrance. Therefore, an alternative approach to this AB model system acetate (−)-**67** was sought and found in a sequence starting with cyclopentanone (−)-**74** (Scheme 12). Thus, aldol reaction of (−)-**74** with acetone through titanium enolate formation ($TiCl_4$, Et_3N, CH_2Cl_2, −78 °C) furnished, exclusively, tertiary alcohol (−)-**80** (92% yield), possessing the expected *anti* stereochemical arrangement between the two substituents flanking its carbonyl group. Stereoselective reduction of this hydroxy ketone with $NaBH_4$ (∼6:1 dr) followed by selective monoacetylation of the resulting diol then furnished hydroxy acetate (−)-**81** (71% yield for the two steps), whose regioselective dehydration with Burgess reagent afforded the desired acetate model system (−)-**67** in 50% yield.

With all eight AB model systems available (**60**−**67**), we were in a position to proceed with the acquisition and analysis of their one-dimensional and two-dimensional NMR spectra. Figure 17 summarizes the crucial coupling constants (*J*-values) and NOEs observed for these compounds. Thus, (+)-**60**, (+)-**61**, (+)-**62**, (−)-**64**, (−)-**65**, and (−)-**67** exhibited relatively large coupling constants for H_6/H_7 ($JH_{6,7}$ = 9.6−11.0 Hz), supporting the *anti* periplanar relationship within these structures [for (+)-**63** and (−)-**66** this coupling constant was not discernible due to signal overlap]. A cursory inspection of the model systems on the left side of Figure 16 (e.g., **60**−**64**) reveals striking similarities between model system (+)-**60** and natural vannusal A. Thus, the coupling constants between H_6/H_7, H_3/H_{29}, and H_{29}/H_6 were the same in the two compounds [$JH_{6,7}$ = 9.6 Hz; $JH_{3,29} = JH_{29,6}$ = 3.5 Hz (t) for both (+)-**60** and natural vannusal A], and so was the chemical shift for H_{29} (δ 5.43 ppm). In addition, model system (+)-**60** exhibited the same NOEs as the natural product. On the other hand, model system (+)-**61** exhibited the diagnostic H_{29} ^{1}H NMR signal as a triplet (δ 5.22 ppm) with a relatively large coupling constant (JH_{29} = 7.8 Hz), the latter being composed of two identical vicinal axial−axial coupling constants $JH_{29,3}$ and $JH_{29,6}$, an occurrence which was further supported by a weak NOE between H_3 and H_6 (1,3-diaxial relationship). Model compounds (+)-**62** and (+)-**63** exhibited significantly different *J*-values for H_{29} [(+)-**62**: dd, *J* = 4.5, 2.0 Hz; (+)-**63**: dd, *J* = 5.4, 1.8 Hz] and, thus, along with (+)-**61**, were excluded as representatives of the true structure of the vannusals. Interestingly, all structures in this series showed one or both of the expected NOEs between H_{29} and $H_{8\alpha}/H_{8\beta}$, an observation that was in line with the original report of such an effect within natural vannusal A.[2]

Shifting our attention to the "right side" series (epimeric at C_6, Figure 17), we noticed a consistent trend among the A-ring *J*-values for H_{29} and H_6/H_7 ($JH_{3,29}$, $JH_{29,6}$, and $JH_{6,7}$) when compared to their "left side" counterparts (see Figure 17). This observation indicated that, despite being diastereoisomers (epimeric at C_6), the structures on the "right side" underwent very little change in the A-ring bond angles/conformation in comparison to those of the "left side" series. We, therefore, felt reasonably comfortable eliminating compounds (−)-**65** (t, $JH_{29,3}/H_{29,6}$ = 9.0 Hz; $JH_{6,7}$ = 9.0 Hz), (−)-**66** (dd, $JH_{29,3}/H_{29,6}$ = 6.0, 3.6 Hz), and (−)-**67** (dd, $JH_{29,3}/H_{29,6}$ = 5.5, 2.5 Hz, $JH_{6,7}$ = 9.6 Hz) on the basis of their diagnostic JH_{29} coupling constants. Interestingly, model compound (−)-**64** was spectroscopically virtually identical to (+)-**60** and the originally assigned structure of vannusal A (see Figure 17) with respect to these coupling constants (although it differed in other aspects of the spectrum). Despite these similarities, (−)-**64**, along with all other members of this series ("right side", Figure 17), lacked the key NOE

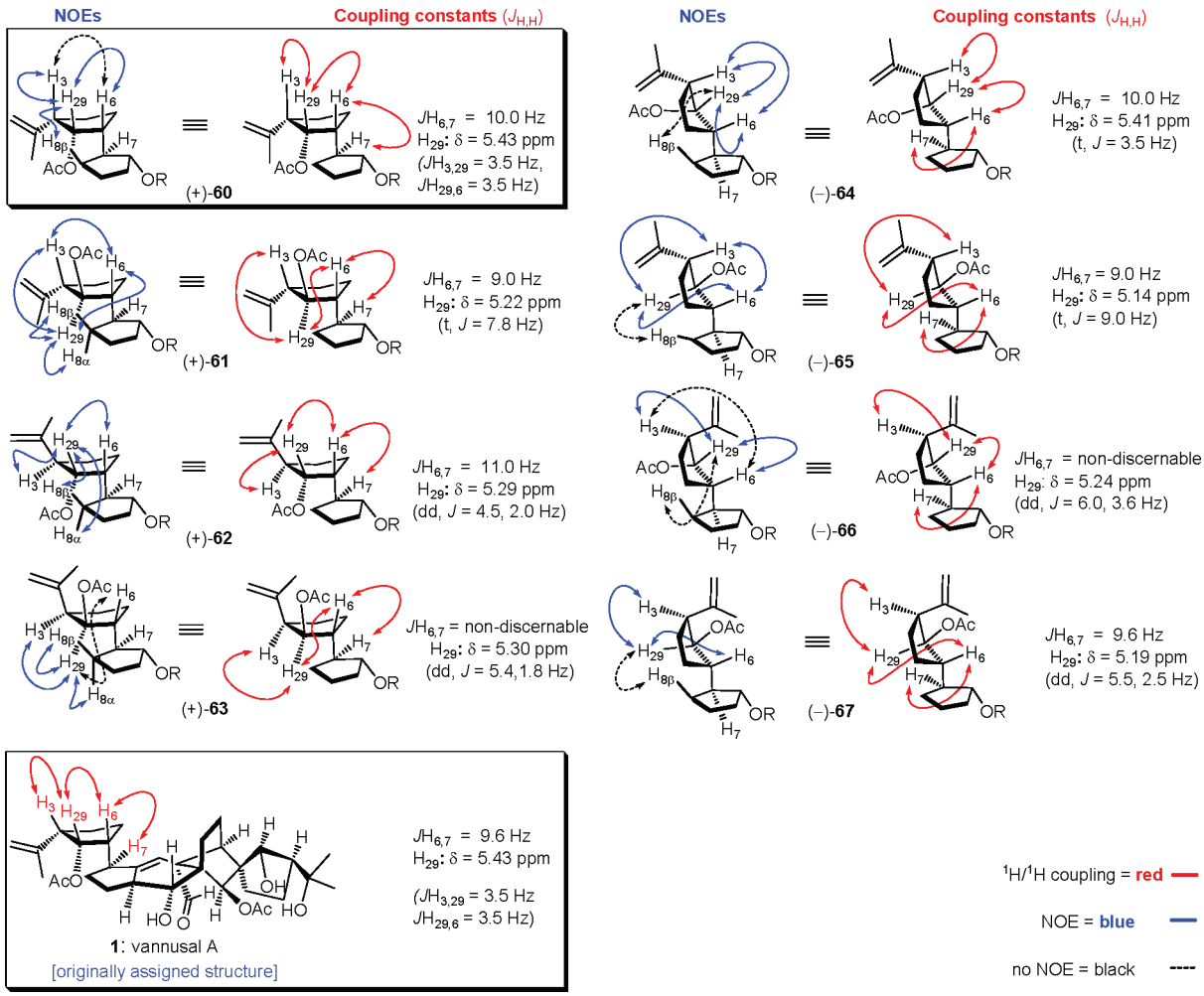

Figure 17. ^1H *J*-coupling constants (red) and NOEs (blue) observed for AB model systems **60**−**67**.

between H_{29} with $H_{8\beta}$, and was consequently eliminated as a suspected representative of the true structure of the vannusals. We had, at this point, removed all of the model compounds of this study from further consideration, with the exception of (+)-**60** (representing the originally assigned structure of the vannusals). While the preceding in-depth spectroscopic analysis led us essentially back to where we had begun (namely the original A-/B-ring structural assignment) it had, nonetheless, laid to rest any further suspicions surrounding this region of the structure of the vannusals.

Total Synthesis of the True Structure of Vannusal B. Having convinced ourselves of the correctness of the "southwestern" domain (i.e., original stereochemical assignments at C_3, C_{29}, C_6, and C_7; rings A and B) through chemical synthesis and spectroscopic analysis, we returned to the "northeastern" region of the vannusal B molecule. Our previous modifications of the vannusal structure pointed to the stereocenters on the E-ring (i.e., C_{25} and C_{21}) as the most likely site of an error, and since we had already synthesized three of the four possible diastereomers of this region of the molecule [i.e., (±)-**84**, (±)-**83**, and (±)-**43**; see Figure 20] and found them not to lead to the true structure of natural vannusal B, the remaining diastereomer [i.e., (±)-**82**, β-C_{25}−OH/α-C_{21}−CMe_2OH, Figure 18] became our next subtarget for the now obligatory NMR spectroscopic analysis. This structure was tentatively rejected earlier as a possible candidate representing the true structure of the natural product on the basis of the rather large coupling constant ($JH_{25,21}$ = 10.0 Hz) exhibited by its opposite counterpart [i.e., (±)-**83**, α-C_{25}−OH/β-C_{21}−CMe_2OH, Figure 18, and the $JH_{25,21}$ = 8.5 Hz exhibited by synthetic vannusal structure B (+)-**3**].

The total synthesis of vannusal B structure (+)-**5** [C_{25}-*epi*-**2**] required, in addition to vinyl iodide (−)-**6**, aldehyde (±)-**94** as a building block containing the "northeastern" domain of the vannusal molecule. The latter precursor could be generated from intermediate (±)-**82**, which was defined as our needed model system for spectroscopic comparison with the other model systems shown in Figure 18 [i.e., (±)-**84**, (±)-**83**, and (±)-**43**]. The syntheses of model system (±)-**82** and aldehyde (±)-**94** are shown in Schemes 13 and 14, respectively. Thus, as already discussed above (see Table 1), diketone (±)-**41** was converted to hydroxy diketone (±)-**85** (~6:1 dr) and subjected to DIBAL-H reduction to afford diastereoselectively triol (±)-**82** (64% yield for the two steps, plus 12% yield of its chromatographically separable C_{21} diastereomer, Scheme 13). Desilylation of (±)-**82** (aq HF, 83% yield) gave crystalline tetraol (±)-**86** (mp 139−141 °C, methanol/benzene), whose X-ray crystallographic analysis (see ORTEP representation, Figure 19)[13] provided unambiguous proof of its structure, and, thereby, its precursor (±)-**82**. The selectivity of the DIBAL-H reduction of hydroxy diketone (±)-**85** (see Scheme 13 and Figure 20) is interesting, especially when compared to the reduction of its TES-protected counterpart [(±)-**87**][1,3] (see Figure 20) that led to the opposite C_{25} configuration (see Figure 20)[1,3] and C_{21} diastereomer [(±)-**42**, see Scheme 7 and Figure 20]. To explain these observations, as well as the reduction of the TES-protected

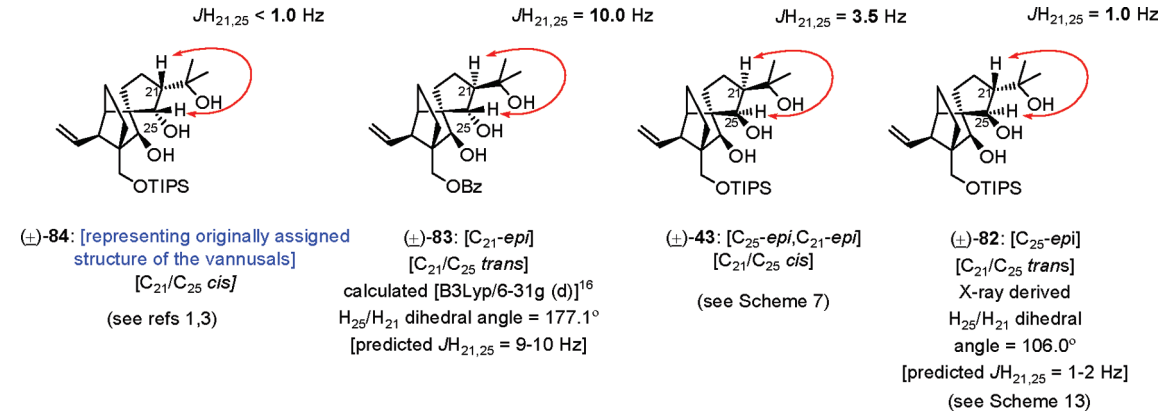

Figure 18. Comparison of the $JH_{21,25}$ coupling constants of DE model systems (±)-**82**, (±)-**83**, (±)-**43**, and (±)-**84**.

Scheme 13. Construction of Triol (±)-**82** and Tetraol (±)-**86**[a]

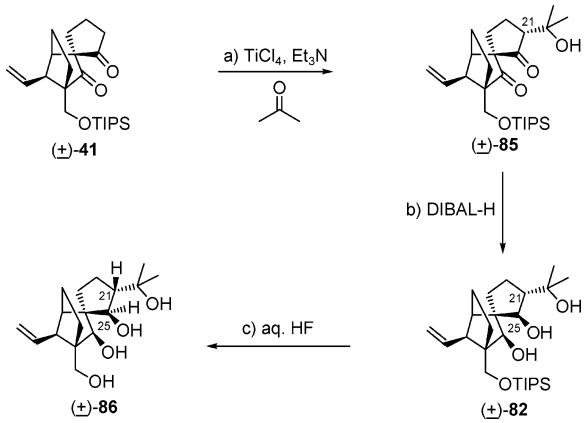

[a] Reagents and conditions: (a) $TiCl_4$ (1.0 M in CH_2Cl_2, 1.2 equiv), Et_3N (3.0 equiv), CH_2Cl_2, −78 → −30 °C, 30 min; then acetone (10 equiv), −78 °C, 8 h (~6:1 dr); (b) DIBAL-H (5.0 equiv), toluene, −78 → °C, 30 min, 64% for the two steps; (c) aq HF/THF (1:4), 25 °C, 18 h, 83%.

version of (±)-**85** (i.e., compound (±)-**87**, see refs 1 and 3 and Figure 20), we postulate hypothetical transition states **85-TS**, **42-TS**, and **87-TS**, respectively. Thus, while the reduction of the C_{26} carbonyl group occurs in all three cases from the opposite side of the C_{15}/C_{16} bridgehead, purely on steric grounds (as expected), the diastereoselectivity of the reduction of the C_{25} carbonyl varies with the substrate/reagent combinations. With substrate (±)-**87** and $NaBH_4$, this reduction occurs from the opposite side of the bulky C_{21} substituent [(±)-**87** → **87-TS** → **84-TES** → (±)-**84**, see Figure 20a], as is the case for substrate (±)-**42** [(±)-**42** → **42-TS** → **43-TES** → (±)-**43**, see Figure 20b]. To explain the opposite diastereoselectivity of the reduction of hydroxy diketone (±)-**85**, we called upon likely dimeric aggregates of DIBAL-H in nonpolar (noncoordinative) media[14] and initial aluminate formation at the hydroxyl group to form transition **85-TS** (Figure 20c). Intramolecular delivery of hydride from the α-face is then possible to generate **82-*i*-Bu$_2$Al**, whose hydrolysis would lead to the observed diastereomeric triol (±)-**82**.

Scheme 14. Construction of Aldehyde (±)-**94**[a]

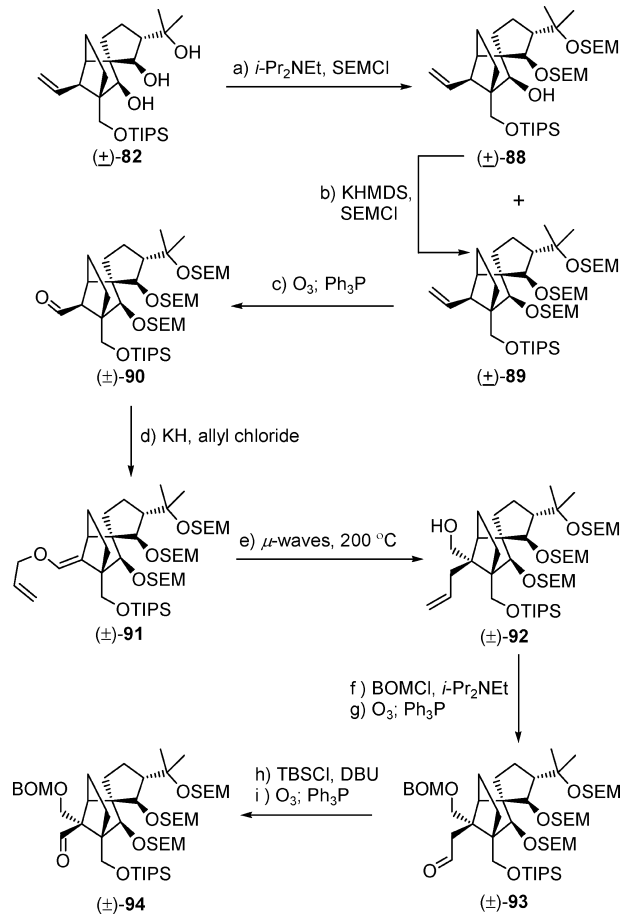

[a] Reagents and conditions (a) *i*-Pr_2NEt (20 equiv), SEMCl (6.0 equiv), *n*-Bu_4NI (1.0 equiv), 50 °C, 24 h; (b) KHMDS (2.0 equiv), SEMCl (5.0 equiv), Et_3N (10 equiv), THF, −78 → 25 °C, 1 h, 96% for the two steps; (c) O_3, py (1.0 equiv), CH_2Cl_2/MeOH (1:1), −78 °C; then Ph_3P (5.0 equiv), −78 → 25 °C, 1 h, 97%; (d) KH (10 equiv), allyl chloride (30 equiv), HMPA (10 equiv), DME, −10 → 25 °C, 8 h, 95%; (e) *i*-Pr_2NEt (1.0 equiv), 1,2-dichlorobenzene, μ-waves, 200 °C, 20 min; then $NaBH_4$ (10 equiv), MeOH, 1 h, 25 °C, 88% for the two steps; (f) BOMCl (10 equiv), *i*-Pr_2NEt (30 equiv), *n*-Bu_4NI (1.0 equiv), CH_2Cl_2, 50 °C 12 h; (g) O_3, py (1.0 equiv), CH_2Cl_2/MeOH (1:1), −78 °C; then Ph_3P (5.0 equiv), −78 → 25 °C, 1 h, 81% for the two steps; (h) TBSCl (10 equiv), DBU (20 equiv), CH_2Cl_2, 25 °C, 12 h; (i) O_3, py (1.0 equiv), CH_2Cl_2/MeOH (1:1), −78 °C; then Ph_3P (5.0 equiv), −78 → 25 °C, 1 h, 80% for the two steps.

(13) CCDC-726955 contains the supplementary crystallographic data for tetraol (±)-**86**. This data can be obtained free of charge from the Cambridge Crystallographic Data Centre via www.ccdc.cam.ac.uk/data_request/cif.

(14) DIBAL-H is known to exist in dimeric and forms in benzene, see: (a) Clark, G. M.; Zweifel, G. *J. Am. Chem. Soc.* **1971**, *93*, 527–528. (b) Ziegler, K.; Kroll, W. R.; Larbig, W. *Justus Liebigs Ann. Chem* **1960**, *629*, 222.

(15) (a) Kock, M. J.; Grube, A.; Seiple, I. B.; Baran, P. S. *Angew. Chem., Int. Ed.* **2007**, *46*, 6586–6594. (b) Smith, S. G.; Paton, R. S.; Burton, J. W.; Goodman, J. M. *J. Org. Chem.* **2008**, *73*, 4053–4062. (c) Wu, A.; Cremer, D. *Int. J. Mol. Sci* **2003**, *4*, 158–192. (d) Sheldrake, H. M.; Jamieson, H. M.; Burton, J. W. *Angew. Chem., Int. Ed.* **2006**, *45*, 7199–7202.

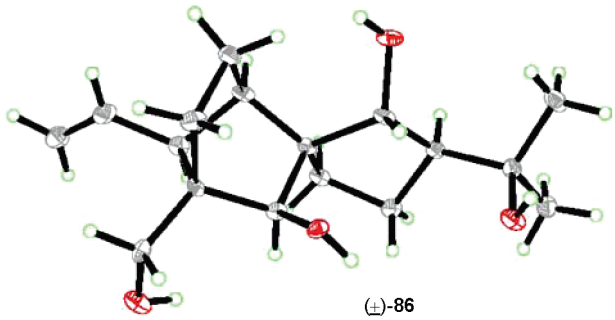

Figure 19. X-ray-derived ORTEP of tetraol (±)-**86**.

^{1}H NMR spectroscopic analysis of the DE ring systems (±)-**82**, (±)-**43**, (±)-**83**, and (±)-**84** revealed interesting coupling constants for H_{25} and H_{21} ($J_{H25,21}$) as shown in Figure 18. Thus, while the two *cis* compounds [(±)-**43** and (±)-**84**] exhibited relatively small coupling constants for these protons [(±)-**43**: $J_{H25,21}$ = 3.5 Hz; (±)-**84**: $J_{H25,21}$ < 1.0 Hz], the two *trans* isomers [(±)-**82** and (±)-**83**] differed drastically in their $J_{H25,21}$ coupling constants, with the latter exhibiting a relatively large value [(±)-**83**: $J_{H25,21}$ = 10.0 Hz] and the former a very small value [(±)-**82**: $J_{H25,21}$ = 1.0 Hz]. The dramatic difference in these coupling constants, although surprising at first, could be understood from the dihedral angles for H_{25}/H_{21} within tetraol (±)-**86** (106.0°) as revealed by X-ray crystallographic analysis of this compound (see ORTEP, Figure 19)[13] and the calculated dihedral angle (177.1°)[16] corresponding to compound (±)-**83**. It also underscored once again the difficulties in determining stereochemical relationships of substituents situated on cyclopentane rings.[15]

Returning to the mainstream synthetic route, the now plentiful triol (±)-**82** served well as a precursor to the targeted aldehyde, fragment (±)-**94**. As shown in Scheme 14, our attempt to prepare the next intermediate, tris-SEM ether (±)-**89**, under the standard conditions (SEMCl, *i*-Pr_2NEt, *n*-Bu_4NI, 50 °C) slowed down at the bis-SEM ether (±)-**88** stage [79% yield, plus 20% yield of (±)-**89**] and had to be pushed forward by resubjecting the chromatographically separable bis-SEM ether to further reaction under more forcing conditions (KHMDS, SEMCl, −78 → 25 °C, (±)-**89**, 96% total yield from (±)-**82**]. The remaining steps from (±)-**89** to aldehyde (±)-**94** proceeded along the previously devised route and through intermediates (±)-**90**−(±)-**93** as summarized in Scheme 14.

With both fragments [(−)-**6** and (±)-**94**] readily available, their union and further elaboration proceeded as shown in Scheme 15. Thus, lithiation of (−)-**6** (*t*-BuLi, THF, −78 → −40 °C), followed by addition of aldehyde (±)-**94** (−40 → 0 °C), led, upon desilylation (TBAF), to chromatographically separable diastereomeric adducts (−)-**95** and (+)-**96** in 84% total yield (~1:1 ratio). Each diastereomer [(−)-**95** and (+)-**96**] was then converted separately to the desired cyclization precursor [(−)-**99** and (+)-**100**, respectively] through the corresponding intermediate hydroxy carbonate [(−)-**97** and (+)-**98**, respectively] by the high-yielding, four-step sequence previously developed and as summarized in Scheme 15 [(i) temporary silylation of the primary alcohol (TESCl, imid.); (ii) carbonate formation at the secondary hydroxyl position (KHMDS, $ClCO_2Me$, Et_3N); (iii) removal of the TES group (HF·py, (−)-**97**: 89% overall yield; (+)-**98**: 96% overall yield); and (iv) oxidation [$PhI(OAc)_2$, AZADO (cat.), (−)-**99**, 96% yield; (+)-**100**, 97% yield].

Our attempts to advance aldehyde carbonate (−)-**99** through the SmI_2-induced cyclization step (see Scheme 16) were thwarted by its resistance to undergo the desired reaction, thus

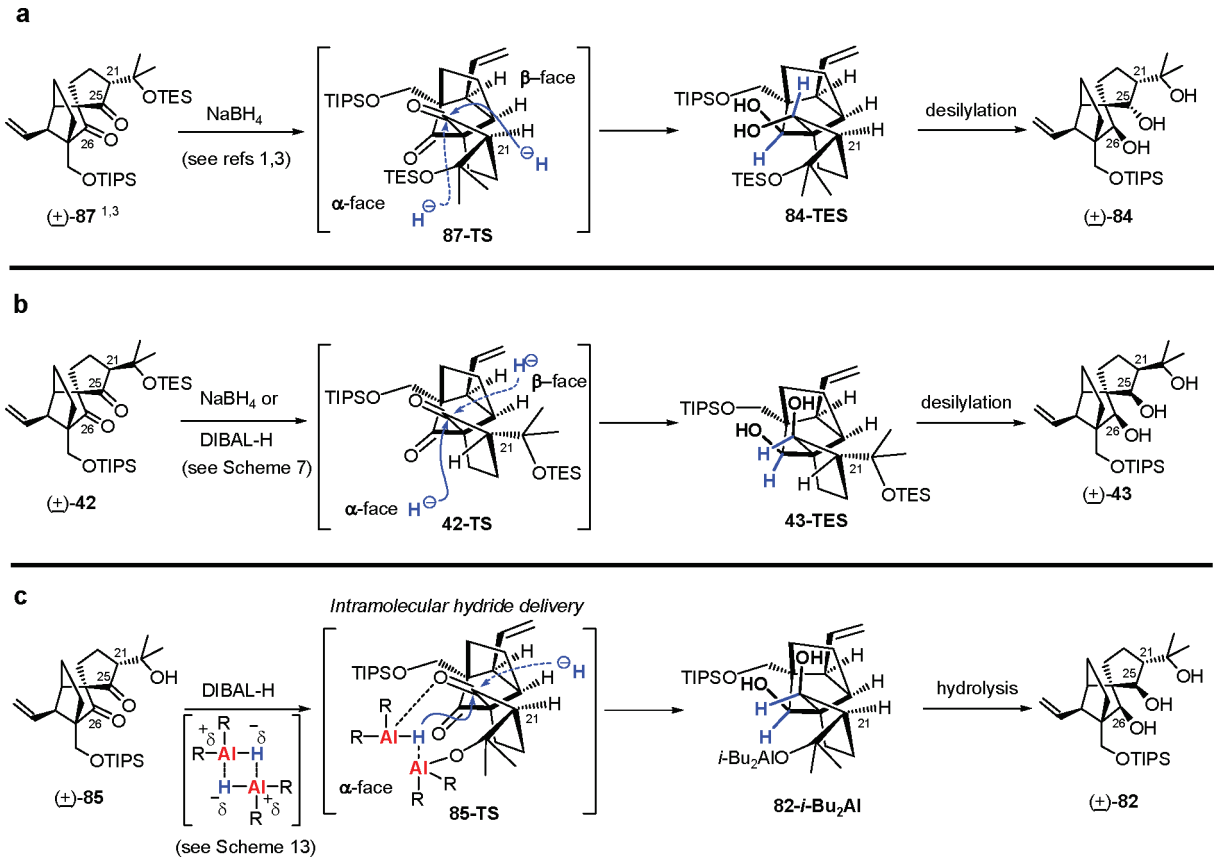

Figure 20. Mechanistic rationale for the diastereoselectivities observed in the reductions of diketones (±)-**42** (a), (±)-**87** (b), and (±)-**85** (c).

Scheme 15. Synthesis of Aldehyde Carbonates (−)-**99** and (+)-**100**[a]

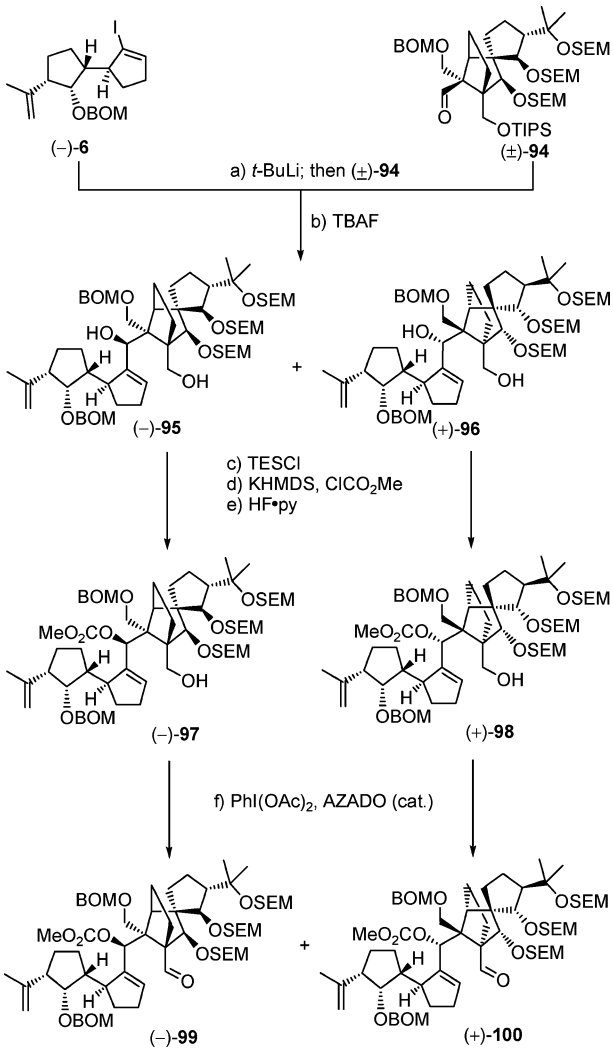

[a] Reagents and conditions: (a) (−)-**6** (1.3 equiv), *t*-BuLi (2.6 equiv), THF, −78 → −40 °C, 40 min; then (±)-**94** (1.0 equiv), −40 → 0 °C, 20 min; (b) TBAF (1.0 M in THF, 2.0 equiv), THF, 25 °C, 8 h, 84% (~1:1 dr) for the two steps, (−)-**95** and (+)-**96** chromatographically separated; c) TESCl (2.0 equiv), imidazole (10 equiv), CH_2Cl_2, 25 °C, 30 min; (d) KHMDS (10 equiv), $ClCO_2Me$ (20 equiv), Et_3N (20 equiv), THF, −78 → 25 °C, 30 min; (e) HF•py/py (1:4), 0 → 25 °C, 12 h, 89% for sequence (−)-**95** → (−)-**97**; 96% for sequence (+)-**96** → (+)-**98** over the three steps; (f) $PhI(OAc)_2$ (2.0 equiv), AZADO (0.1 equiv), CH_2Cl_2, 25 °C, 24 h, 96% for (−)-**99**, 97% for (+)-**100**.

forcing us to deviate slightly from our plans. Suspecting steric congestion with this particular substrate, we explored the removal of one or more of its SEM groups. To this end, we treated (−)-**99** with aq HF in THF, and much to our delight observed selective removal of two of its SEM groups to afford cleanly dihydroxy SEM derivative (−)-**101**, in which the lone SEM group resided on the C_{25} oxygen as determined by ^1H NMR spectroscopic analysis (that revealed an NOE between H_{25} and one of the methylene acetal protons of the SEM group). It was with some trepidation that we exposed the newly prepared cyclization precursor to the SmI_2 conditions (due to the presence of the two hydroxyl groups and the absence of the C_{26}—SEM group that proved beneficial in previous occasions). Pleasantly,

Scheme 16. Samarium Diiodide Cyclization Results for Aldehyde Carbonates (−)-**99** and (−)-**101**[a]

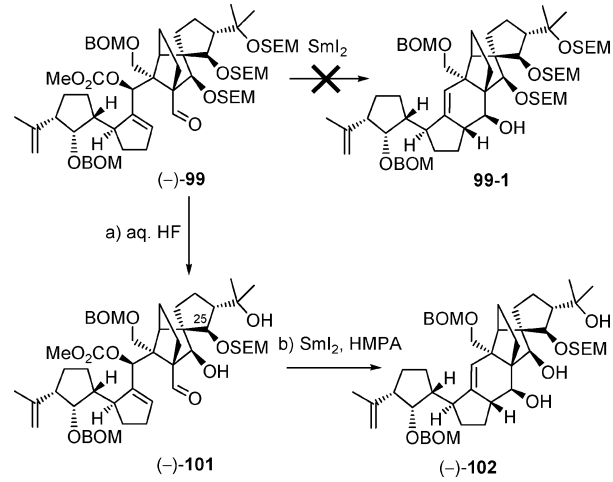

[a] Reagents and conditions: (a) aq HF/THF (1:4), 25 °C, 1.5 h, 81%; (b) SmI_2 (0.1 M in THF, 10 equiv), HMPA (30 equiv), THF, −20 → 25 °C, 20 min, 67%.

however, the reaction proceeded well, furnishing polycyclic product (−)-**102** in 67% yield as a single diastereomer.

Having secured polycyclic intermediate (−)-**102** we then turned our attention to its conversion to the targeted vannusal B structure **5** (Scheme 17). The first task was the inversion of the configurations at C_{10} and C_{28} through the previously developed procedure involving xanthate formation followed by Chugaev elimination. To this end, selective acetylation of (−)-**102** (Ac_2O, 4-DMAP, Et_3N, quant.) led to monoacetate (−)-**103**, whose exposure to standard SEM ether-forming conditions (SEMCl, *i*-Pr_2NEt, CH_2Cl_2, 50 °C) resulted in reaction at the C_{22} hydroxyl, but not the apparently less reactive C_{26} hydroxyl group, to afford the corresponding bis-SEM derivative from which the acetate group was removed through the action of DIBAL-H leading to diol (−)-**104** (83% yield for the two steps). The observed relatively large coupling constant between H_{10} and H_{28} ($J_{H10,28}$ = 7.5 Hz) in (−)-**103** confirmed the *trans* (axial−axial) relationship of these protons within this structure, thus providing support for the structures of both (−)-**103** and (−)-**102**. Reaction of compound (−)-**104** with NaH, first in the presence of CS_2 and then MeI, resulted in selective xanthate formation at C_{28} in 79% yield. Heating of this xanthate at 185 °C (microwave conditions) led to the corresponding conjugated diene (88% yield),[10] whose remaining hydroxyl group was capped with a SEM group under the more forcing conditions of KHMDS−SEMCl−Et_3N (78% yield) to afford tri-SEM derivative (+)-**105**. Sequential hydroboration/oxidation of the latter ($ThexBH_2$; BH_3; H_2O_2, NaOH, 71% yield), followed by selective aryl selenylation of the resulting diol (*o*-$NO_2C_6H_4SeCN$, *n*-Bu_3P) and oxidation/*syn*-elimination (H_2O_2, 86% overall yield for the two steps),[11] gave the desired hydroxy compound (−)-**106**, possessing the correct configuration at both C_{10} and C_{28}. TES protection of (−)-**106** (TESCl, KHMDS, 93% yield) followed by cleavage of the BOM groups (LiDBB, 85% yield) furnished diol (−)-**107**, whose primary hydroxyl moiety was selectively oxidized with $PhI(OAc)_2$ in the presence of TEMPO to afford the corresponding hydroxy aldehyde in 88% yield. Subsequent acetylation of the latter (Ac_2O, 4-DMAP, quant.) led to aldehyde acetate (+)-**108**. Finally, exposure of (+)-**108** to aq HF caused cleavage of all four silicon groups, leading to vannusal B structure (+)-**5**. The total synthesis of this coveted structure was completed shortly after we arrived at

(16) Frisch, M. J.; et al.; *Gaussian 03*; Gaussian, Inc.: Wallingford CT, 2004.

Scheme 17. Total Synthesis of Vannusal B Structure (+)-**5** [C_{25}-*epi*-**2**][a]

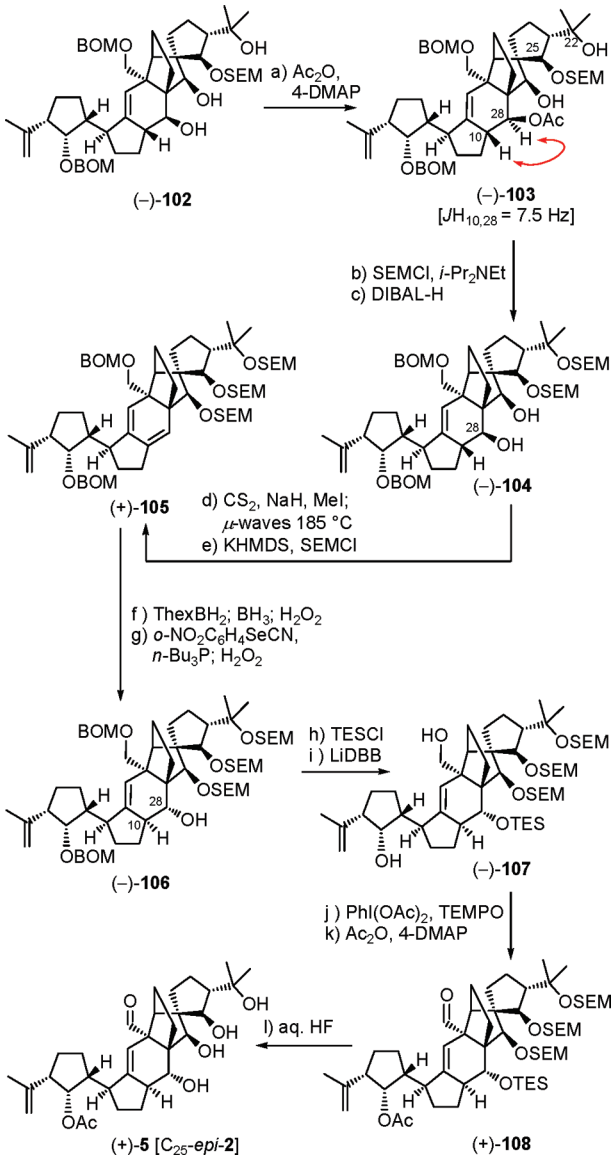

[a] Reagents and conditions: (a) Ac_2O (20 equiv), Et_3N (20 equiv), 4-DMAP (0.2 equiv), CH_2Cl_2, 25 °C, 30 min, quant.; (b) SEMCl (10 equiv), *i*-Pr_2NEt (30 equiv), CH_2Cl_2, 50 °C, 18 h; (c) DIBAL-H (5.0 equiv), CH_2Cl_2, −78 °C, 30 min, 83% for the two steps; (d) NaH (4.0 equiv), CS_2 (2.3 equiv), THF, 0 → 25 °C, 30 min; then MeI (4.6 equiv), 0 → 25 °C, 1 h, 79%; then μ-waves, 185 °C, 1,2-dichlorobenzene, 15 min, 88%; (e) KHMDS (4.0 equiv), SEMCl (4.0 equiv), Et_3N (8.0 equiv), THF, −50 → 25 °C, 20 min, 78%; (f) $ThexBH_2$ (5.0 equiv), THF, −10 → 25 °C, 30 min; then BH_3·THF (15 equiv), 25 °C, 1 h; then 30% H_2O_2/3 N aq NaOH (1:1), 25 → 45 °C, 30 min; 71% (1:1.3 dr); (g) *o*-$NO_2C_6H_4SeCN$ (3.0 equiv), *n*-Bu_3P (9.0 equiv), py (12 equiv), THF, 25 °C, 10 min; then 30% H_2O_2, 25 → 45 °C, 30 min, 86%; (h) KHMDS (6.0 equiv), TESCl (4.0 equiv), Et_3N (8.0 equiv), THF, −50 → 25 °C, 20 min, 93%; (i) LiDBB (excess), THF, −78 → −50 °C, 30 min, 85%; (j) $PhI(OAc)_2$ (4.0 equiv), TEMPO (2.0 equiv), CH_2Cl_2, 25 °C, 15 h, 88%; (k) Ac_2O (30 equiv), Et_3N (60 equiv), 4-DMAP (2.0 equiv), CH_2Cl_2, 25 °C, 24 h, quant.; (l) aq HF/THF (1:3), 25 °C, 6 h, 90%.

its diastereomer **d-5**, whose total synthesis from diastereomeric aldehyde carbonate (+)-**100** we describe next (see Scheme 18).

As events transpired, the total synthesis of vannusal B structure (+)-**d-5** turned out to be considerably shorter than the one leading to the initially targeted vannusal B structure (+)-**5**. Thus, reaction of (+)-**100** with SmI_2 in THF in the presence of HMPA at −20 → 25 °C furnished, much to our delight, a single

Scheme 18. Total Synthesis of Vannusal B Structure (+)-**d-5** [C_{25}-*epi*-**d-2**][a]

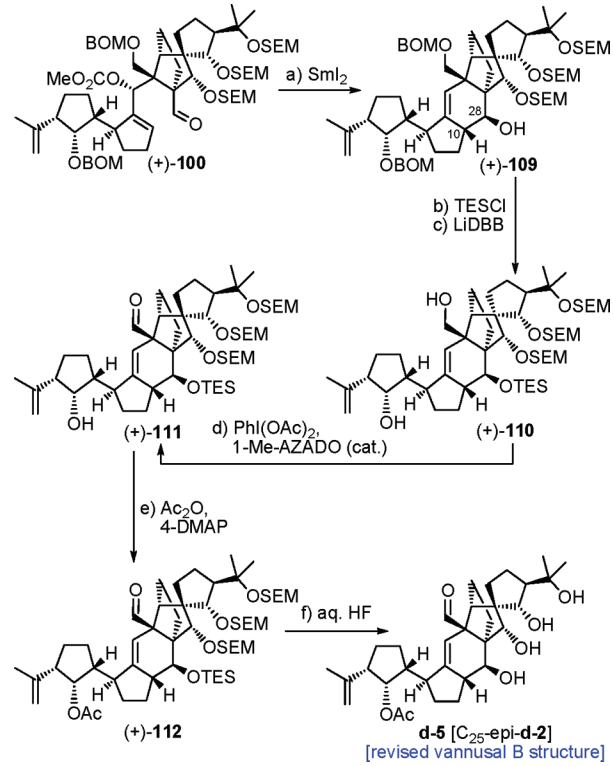

[a] Reagents and conditions: (a) SmI_2 (0.1 M in THF, 10 equiv), HMPA (30 equiv), THF, −20 → 25 °C, 30 min, 82%; (b) KHMDS (5.0 equiv), TESCl (10 equiv), Et_3N (10 equiv), THF, −78 → 25 °C, 20 min, 94%; (c) LiDBB (excess), THF, −78 → −50 °C, 30 min, 83%; (d) $PhI(OAc)_2$ (2.0 equiv), 1-Me-AZADO (0.2 equiv), CH_2Cl_2, 25 °C, 18 h; (e) Ac_2O (10 equiv), Et_3N (20 equiv), 4-DMAP (1.0 equiv), CH_2Cl_2, 25 °C, 18 h, 87% for the two steps; (f) aq HF/THF (1:3), 25 °C, 3 h, 85%.

diastereomeric product (+)-**109** and in 82% yield (see Scheme 18). Equally pleasing was the realization that this product possessed the correct configuration at C_{10}/C_{28} relative to the rest of the "northeastern" (but not to the "southwestern") region of the molecule and, as such, needed no further configurational adjustments, as its diastereomer (i.e., (+)-**5** Scheme 17) did. Consequently, only a five-step sequence was standing between intermediate (+)-**109** and the final product, vannusal B structure (+)-**d-5**. Thus, TES installment at the C_{28} hydroxyl group (TESCl, KHMDS, 94%) followed by LiDBB-induced removal of the BOM groups led to diol (+)-**110** (83% yield), whose selective oxidation [$PhI(OAc)_2$, 1-Me-AZADO (cat.)][9] of the primary hydroxyl group furnished hydroxy aldehyde (+)-**111**. Subsequent acetylation of the remaining secondary hydroxyl group within the latter intermediate afforded polysilylated acetoxy aldehyde (+)-**112** (87% for the two steps), whose desilylation with aq HF led to vannusal B structure (+)-**d-5** in 85% yield.

The 500 MHz ^{1}H NMR spectrum of synthetic (+)-**d-5** was consistent with its structure, but even more pleasing was its remarkable similarity to that of natural vannusal B, which happened to be a 600 MHz spectrum.[2] Reasoning that this favorable comparison meant that we were getting closer to the real structure of the vannusals, our anticipation for synthetic vannusal B structure (+)-**5** was heightened. Our excitement, however, was abruptly quenched shortly thereafter when we arrived at the latter, whose 600 MHz NMR spectrum, although consistent with its structure, did not match the 600 MHz ^{1}H

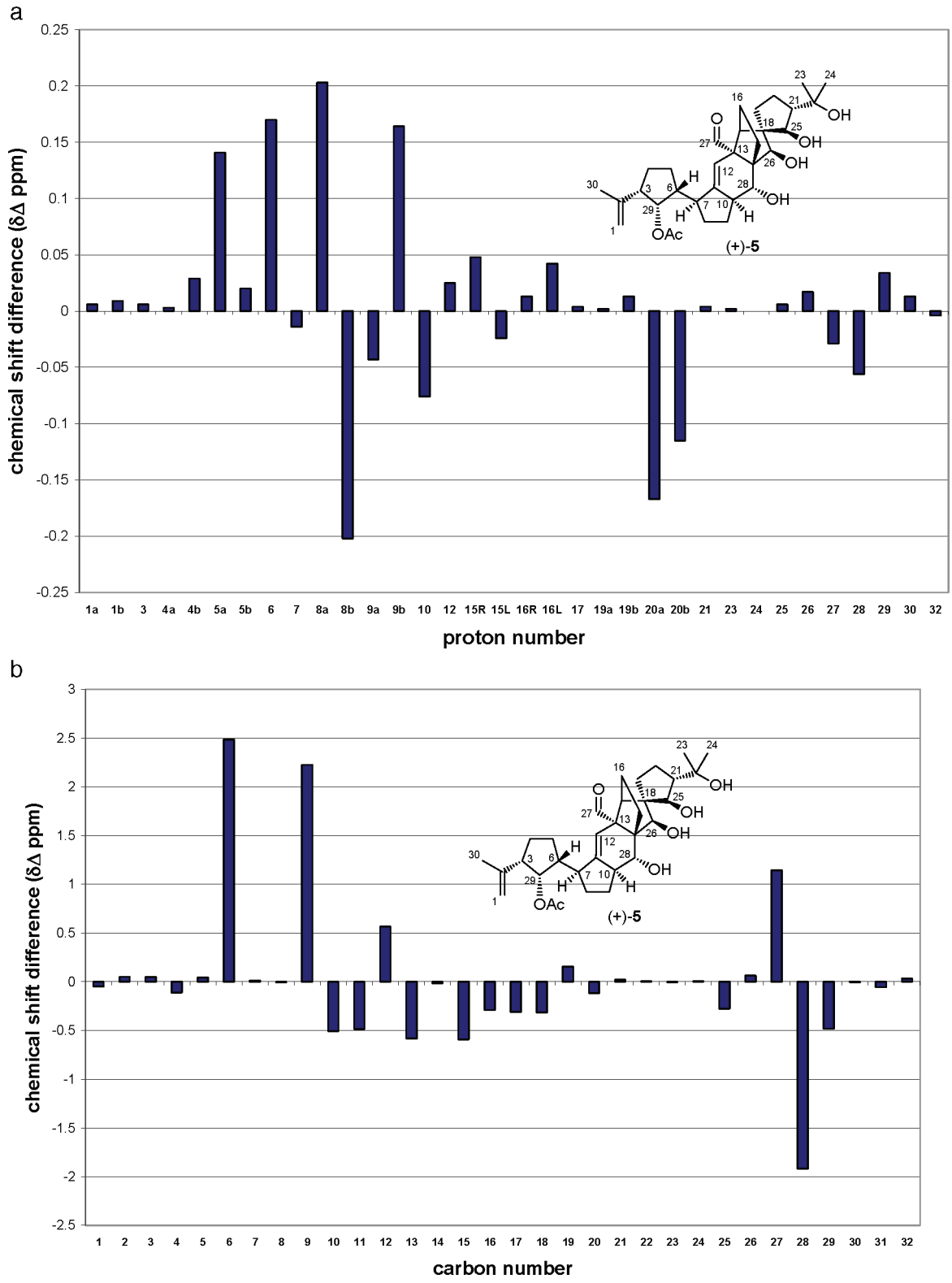

Figure 21. (a) Graphically depicted ^{1}H NMR chemical shift differences ($\Delta\delta$, ppm, d_4-MeOH, 600 MHz) between vannusal B structure [(+)-**5**] and natural vannusal B (set to zero). (b) Graphically depicted ^{13}C NMR chemical shift differences ($\Delta\delta$, ppm, d_4-MeOH, 600 MHz) between vannusal B structure [(+)-**5**] and natural vannusal B (set to zero).

NMR spectrum of natural vannusal B.[2] Panels a and b of Figure 21 respectively demonstrate the ^{1}H and ^{13}C NMR chemical shift differences between vannusal B structure (+)-**5** (red bars) and natural vannusal B (set to zero). Interestingly, the majority of the ^{1}H and ^{13}C NMR inconsistencies are located in the ABC ring ("southwestern") segment (an occurrence that can be more easily rationalized when comparing the structure of (+)-**5** with the revised structure of vannusal B revealed below).

Thankfully, our disappointment was only short-lived, for it was almost immediately that we returned to structure (+)-**d-5**, this time securing its 600 MHz NMR spectrum for a more reliable comparison with the corresponding spectrum of the

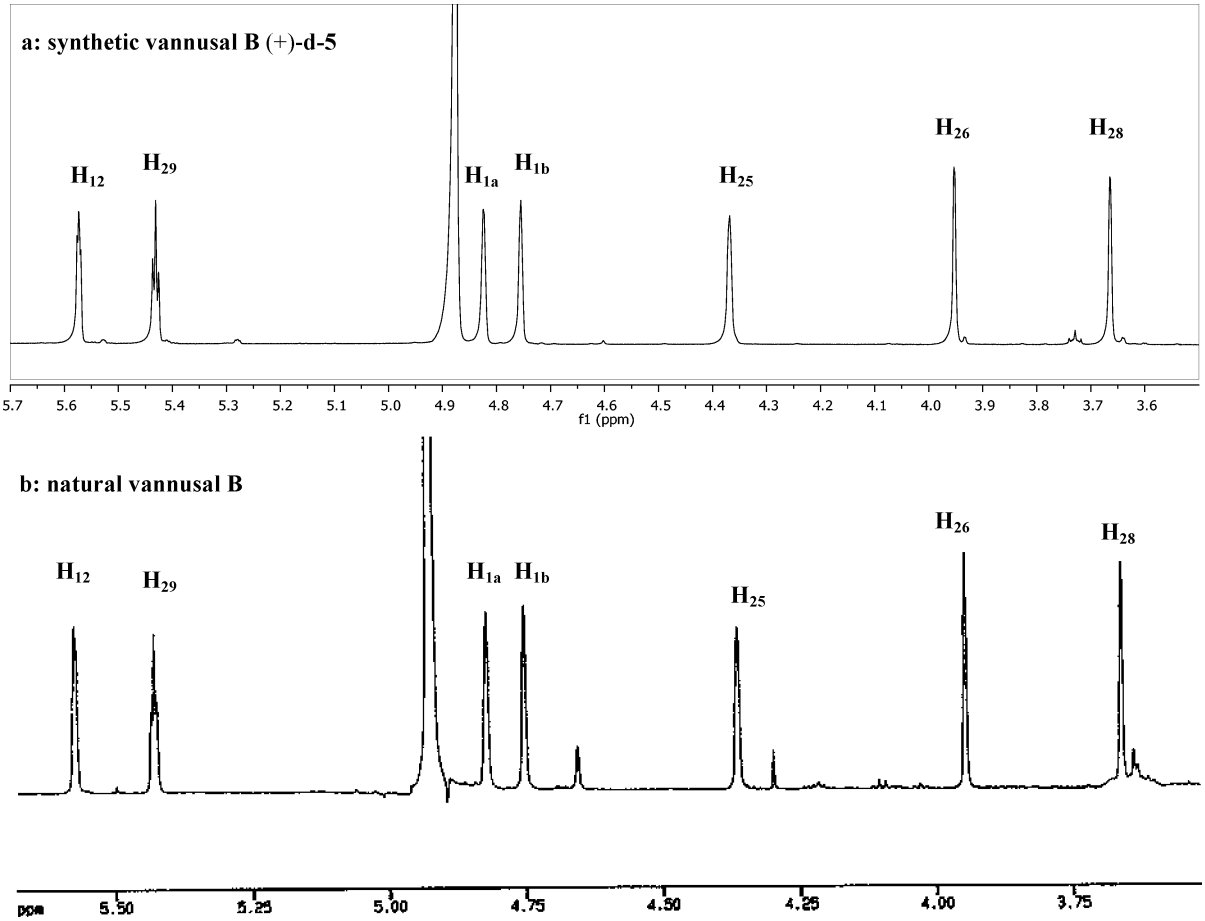

Figure 22. ^{1}H NMR spectral comparison (δ 5.7−3.5 ppm, d_4-MeOH, 600 MHz) of synthetic vannusal B structure [(+)-**d-5**] (a) and natural vannusal B (b).

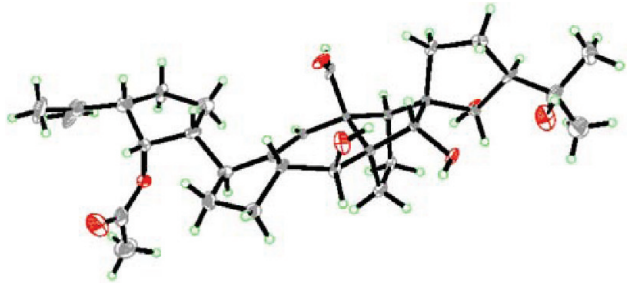

Figure 23. X-ray derived ORTEP of synthetic vannusal B [(+)-**d-5**)].

natural product.[2] Indeed, the two spectra were identical in all respects (see Figure 22 for the diagnostic region δ 5.7−3.5 ppm), and so were its other physical properties including its ^{13}C NMR and MS spectra. The CD spectrum of synthetic (+)-**d-5** [λ [nm] = 229 (+20.15), 308 (−12.03)] was identical to that reported for natural vannusal B [λ [nm] = 229 (+5.4), 308 (−3.1)], thus confirming the absolute configuration of natural vannusal B as presented in structure (+)-**d-5**.[2] Delightfully, synthetic vannusal B crystallized from EtOAc/THF in beautiful needles (mp >200 °C dec) that yielded to X-ray crystallographic analysis (see ORTEP, Figure 23),[17] providing the ultimate structural proof of this intriguing natural product. With the true structure and total synthesis of vannusal B [(+)-**d-5**)] secured, our next task became the total synthesis of vannusal A, whose originally assigned structure (**1**) was safely revised to structure **d-1** in accordance with the revised structure of its closely related congener, vannusal B [(+)-**d-5**]. Our confidence for the skeletal and configurational identity of the two vannusals (A and B) was based on the similarity of their NMR spectral data and their previous conversion to the same pentaol derivative [(+)-**113**)] by Guella, Pietra, and Dini[2] by $NaBH_4$ reduction, an observation that we confirmed with synthetic vannusal B structure [(+)-**d-5**, see Scheme 19]. The spectral data of synthetic pentaol (+)-**113** were identical to those reported in ref 2.

Total Synthesis of the Revised Structure of Vannusal A. Focusing on the synthesis of vannusal A [(−)-**d-1**)] from vannusal B [(+)-**d-5**], we initially attempted direct acetylation of the latter, but unfortunately we observed no useful selectivity. Nevertheless, these experiments revealed that the most reactive of the four hydroxyl groups within [(+)-**d-5**] was that situated at C_{28} (see Scheme 20). This realization led us to construct the $C_{28}/C_{25}/C_{22}$ tris-TES derivative of vannusal B, but again the attempt to acetylate the remaining hydroxyl group (C_{26}) was thwarted by the resistance of this, apparently crowded, position to undergo the desired acetylation. Faced with this predicament, we reasoned that tethering the C_{25} and C_{22} hydroxyl groups together through a benzylidene-type bridge (e.g., PMP acetal) may result in pulling the tertiary alcohol away from the vicinity of the C_{26} hydroxyl group [see structure (+)-**115**, Scheme 20], thereby increasing the reactivity of the latter moiety. Thus, treatment of vannusal B [(+)-**d-5**] with $PMB(OMe)_2$ and PPTS resulted in the formation of the desired PMP acetal (+)-**115** (60% yield), together with the overprotected mixed acetal (+)-**114**, which could be recycled through acid-induced (aq HCl,

(17) CCDC-726954 contains the supplementary crystallographic data for vannusal B [(+)-**d-5**] and is available from The Cambridge Crystallographic Data Centre free of charge via www.ccdc.cam.ac.uk/data_request/cif.

Scheme 19. Synthesis of Pentaol (+)-**113**[a]

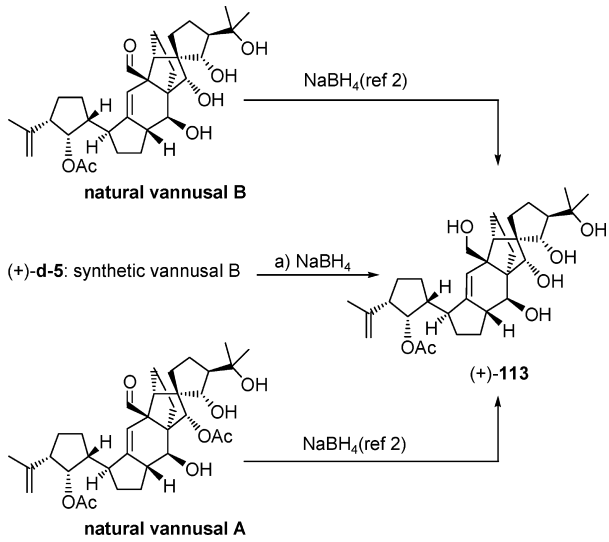

[a] Reagent and conditions: (a) $NaBH_4$ (20 equiv), MeOH, 25 °C, 20 min, 90%.

Scheme 20. Total Synthesis of Vannusal A [(−)-**d-1**][a]

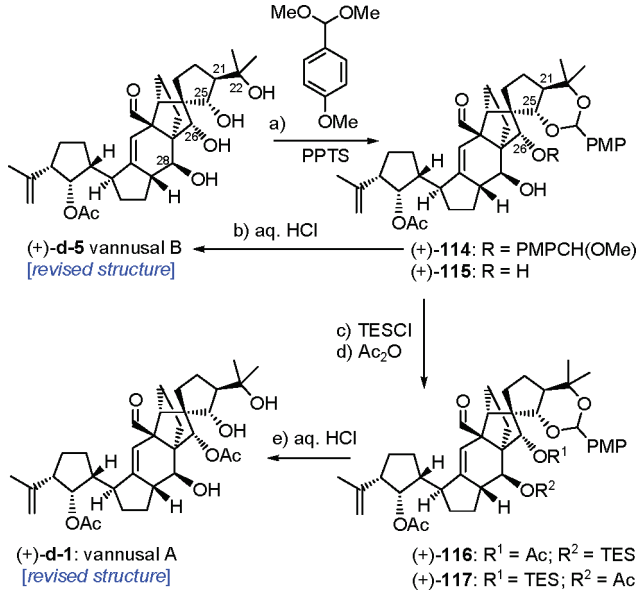

[a] Reagents and conditions: (a) $PMPCH(OMe)_2$ (10 equiv), PPTS (1.0 equiv), DMF, 50 °C, 12 h, (+)-**115**: 60%, (+)-**114**: 22%; (b) 3 N aq HCl, THF, 25 °C, 30 min, 91%; (c) TESCl (10 equiv), imidazole (20 equiv), CH_2Cl_2, 25 °C, 8 h; (d) Ac_2O (20 equiv), 4-DMAP (1.0 equiv), py, 25 °C, 12 h; (e) THF/H_2O (4:1), 12 N aq HCl, 25 °C, 1 h, 43% for the three steps.

91% yield) conversion back to vannusal B [(+)-**d-5**]. Indeed, the predicted conformational change in going from vannusal B to its C_{25}/C_{22} acetal structure was confirmed by the relatively large coupling constant between H_{25} and H_{21} ($J_{H25,21}$ = 12.0 Hz) for acetal (+)-**115** as opposed to the small coupling constant between H_{25} and H_{21} ($J_{H25,21}$ = 2.0 Hz) for vannusal B [(+)-**d-5**] (see Figure 24). As expected, the reactivity of the C_{26} hydroxyl group of diol acetal (+)-**115** increased considerably (as compared to vannusal B), as treatment of the former with TESCl and imidazole followed by acetylation led to a mixture of TES-acetate derivatives (+)-**116** and (+)-**117** [(+)-**116**/(+)-**117** ~1.5:1 ratio]. Exposure of this mixture to aq HCl at ambient temperature furnished, after chromatographic separation, vannusal A [(−)-**d-1**] in 43% overall yield for the three steps. The physical properties of synthetic [(−)-**d-1**] (^{1}H NMR, ^{13}C NMR, $[\alpha]^{25}_D$, and MS) matched those reported for the natural vannusal A.[2] Thus, the true structure of vannusal A was revealed and secured unambiguously as **d-1** (Scheme 20).

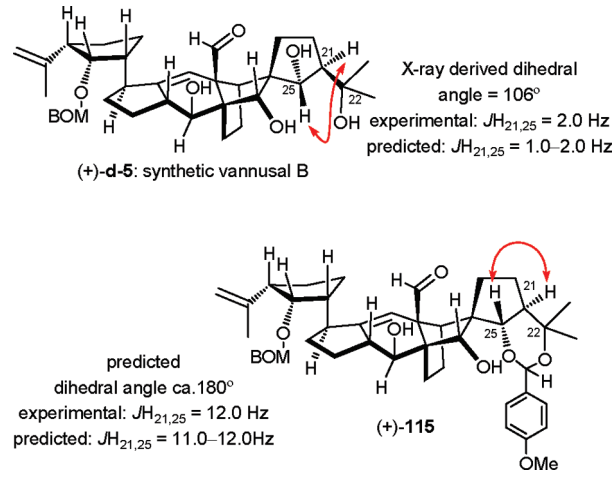

Figure 24. Conformational differences between vannusal B [(+)-**d-5**] and its C_{25}/C_{22}-PMP acetal [(+)-**115**].

Conclusion

Culminating in the total synthesis and structural revision of vannusals A and B, the chemistry described in this and the preceding article[1] demonstrate the power of chemical synthesis to reach complex molecular architectures and its indispensable role in structure elucidation, despite the impressive advances in analytical techniques and instrumentation witnessed in recent times. The employed convergent synthetic strategy to these structures relies on a stereoselective lithium-mediated coupling of a vinyl iodide and an aldehyde, and a SmI_2-induced ring closure involving a formal S_N2' type displacement that expands the scope of this powerful reagent in organic synthesis. As a result of these investigations, these scarce marine natural products and several of their diastereomers are now readily available in their enantiomerically pure forms and in sufficient quantities for biological investigations. Furthermore, the NMR spectroscopic insights gained in these studies underscore the difficulties in relying on coupling constants to assign stereochemical configurations around five-membered rings and provide clues as to how to approach such stereochemical problems. Finally, the strategies and tactics developed in these studies may find useful applications in future chemical synthesis endeavors.

Acknowledgment. We thank Drs. D. H. Huang, G. Siuzdak, and R. Chadha for NMR spectroscopic, mass spectrometric, and X-ray crystallographic assistance, respectively. Financial support for this work was provided by the NSF (fellowship to A.O.), the Skaggs Institute for Research, and grants from the National Institutes of Health (U.S.A.) (GM063752 and CA100101).

Supporting Information Available: Experimental procedures and full compound characterization. This material is available free of charge via the Internet at http://pubs.acs.org.

JA100742B